University of Massachusetts Amherst
ScholarWorks@UMass Amherst

Doctoral Dissertations | Dissertations and Theses

November 2015

From Molecular Scale to Mesoscale: Establishing Structural Control Organic Photovoltaics Using Organic Nanoparticles

Timothy S. Gehan
University of Massachusetts - Amherst

Follow this and additional works at: https://scholarworks.umass.edu/dissertations_2

 Part of the Materials Chemistry Commons, Organic Chemistry Commons, and the Polymer Chemistry Commons

Recommended Citation

Gehan, Timothy S., "From Molecular Scale to Mesoscale: Establishing Structural Control Organic Photovoltaics Using Organic Nanoparticles" (2015). *Doctoral Dissertations*. 507.
https://scholarworks.umass.edu/dissertations_2/507

This Open Access Dissertation is brought to you for free and open access by the Dissertations and Theses at ScholarWorks@UMass Amherst. It has been accepted for inclusion in Doctoral Dissertations by an authorized administrator of ScholarWorks@UMass Amherst. For more information, please contact scholarworks@library.umass.edu.

FROM MOLECULAR SCALE TO MESOSCALE: ESTABLISHING STRUCTURAL CONTROL IN ORGANIC PHOTOVOLTAICS USING ORGANIC NANOPARTICLES

A Dissertation Presented

by

TIMOTHY SEAN GEHAN

Submitted to the Graduate School of the
University of Massachusetts Amherst in partial fulfillment
of the requirements for the degree of

DOCTOR OF PHILOSOPHY

September 2015

Chemistry

© Copyright by Timothy Sean Gehan 2015

All Rights Reserved

FROM MOLECULAR SCALE TO MESOSCALE: ESTABLISHING STRUCTURAL CONTROL ORGANIC PHOTOVOLTAICS USING ORGANIC NANOPARTICLES

A Dissertation Presented

by

TIMOTHY SEAN GEHAN

Approved as to style and content by:

_____
Paul M. Lahti, Co-Chair

_____
Dhandapani Venkataraman, Co-Chair

_____
Michael D. Barnes, Member

_____
E. Bryan Coughlin, Member

_____
Craig T. Martin, Department Head
Department of Chemistry

DEDICATION

This dissertation is dedicated to my family: my father Austin Gehan, my mother Kathleen Gehan, and my brothers Thomas Gehan, Brian Gehan, and Colin Gehan. Without them I would never know what it means to be a good and honorable person, how to love, and how to dedicate yourself to what you believe. I would be lost. They are an endless well of support that has persistently facilitated my growth professionally and personally.

My three brothers are amazing role models and have been, and always will be, my continuous source of inspiration as they embody what it means to be a man. Each one is very unique and extraordinary. They have advised and supported me through every life choice I have made, and I know they will always be there for me through life's highs and lows. I continuously strive to be the man that they believe I can be, and I am immensely thankful every day to have them in my life.

My parents, Austin and Katie, to me are unparalleled life mentors and I could not ask for better parents. They have been resolute and compassionate with their support for me both professionally and personally. I have learned so much from them about being a good and honorable person, how to dedicate yourself to what you believe is right, and how to love. One of their most important lessons that has shaped my life is: "Dedicate yourself to what you love and you will always be successful and happy." I try my best to follow this every day.

Without all of their support and guidance, I know that completing a dissertation would not have been achievable for me. Therefore, this dissertation is entirely dedicated to you.

ACKNOWLEDGMENTS

I would first like to thank my advisors, Professor Paul M. Lahti and Prof. D. Venkataraman, for their guidance and unwavering support. They have shown me, by continuous demonstration, what it means to be a great scientist and a professional. I am eternally grateful for their consistent patience and always encouraging me to become a better scientist and a deep thinker.

I would like to thank my other two dissertation committee members, Prof. Michael Barnes and Prof. E. Bryan Coughlin, for all of their advice and guidance throughout my dissertation. They always pushed me to be a deeper thinker, and I am extremely grateful for that.

I would like to thank all of the Lahti Group members that I had the pleasure to work with. I would especially like to thank Paul Homnick for teaching me how to be an effective synthetic organic chemist.

I would like to thank all of the DV Group members that I was lucky enough to work with. They all have been very supportive, and truly understand the values of working as a team. Dr. Monojit Bag deserves a very special acknowledgment as we worked very closely together on a lot of the work described in this dissertation. We made a great team pairing his physics and device knowledge with my chemistry and molecular understanding. He collected all of the time-of-flight charge mobility data, organic photovoltaic device performance data, and helped with the nanoparticle film preparation. I would also like to acknowledge Dana D. Algaier for collecting some of the scanning electron micrographs, and transmission electron micrographs. I would like to acknowledge Lawrence A. Renna for collecting all of the atomic force

microscopy data (including the conducting AFM data), performing the simulations of random binary nanoparticle assemblies, and collecting the x-ray diffraction data.

I would like to thank Prof. Thomas Russell and his group for all of the collaboration and great discussions. I would like to acknowledge Xiaobo Shen for collecting some of the scanning electron microscopy data, Fen Liu for collecting the grazing incidence x-ray scattering data, and Sunzida Ferdous for teaching me how to use the slot-die coater.

I would like to thank Prof. Dimitrios Maroudas and Xu Han for our great collaboration on further understanding the charge transport through nanoparticle assemblies and organic nanoparticle photovoltaic devices by modeling them.

I would like to thank Prof. Anthony Dinsmore and Yipeng Yang for great discussions on nanoparticle assembly and understanding charge transport through P3HT nanoparticle assemblies.

I would like to thank Prof. Vincent Rotello, Dr. Vikas Nandwana, and Ziwen Jiang for discussions and collaborating on ink-jet printing these organic nanoparticle devices.

I would like to thank Mr. Robert Praino from Chasm Technologies for mentoring me on scaling up thin film devices using nanomaterials.

I would like to thank the DOE PHaSE EFRC for funding during my PhD, and for creating a great atmosphere for collaboration. I would like to thank the OCTV for partially funding this work. I would like to thank Eugene and Ronnie Isenberg and the Isenberg professors for awarding me the Isenberg Scholarship. I would also like to thank Paul Manning, the college of natural sciences administration, and the

technology transfer office for awarding me the Manning Inventor Postdoctoral Fellowship to scale up the technology described in this dissertation.

Finally I would like to thank all of my friends during graduate school, as they have been an amazing support system. We have had a lot of fun as grad students, and I am very thankful every day that I have so many amazing people I get to call "Friend".

ABSTRACT

FROM MOLECULAR SCALE TO MESOSCALE: ESTABLISHING STRUCURAL CONTROL IN ORGANIC PHOTOVOLTAICS USING ORGANIC NANOPARTICLES

SEPTEMBER 2015

TIMOTHY SEAN GEHAN, B.S., SIENA COLLEGE

B.S., RENSSELAER POLYTECHNIC INSTITUTE

Ph.D., UNIVERSITY OF MASSACHUSETTS AMHERST

Directed by: Professor Paul M. Lahti and Professor D. Venkataraman

Organic photovoltaic devices use an active layer of organic materials that absorbs light and creates free charges to generate electricity. Such organic photovoltaics have many desirable properties as the final devices can be very lightweight, thin, flexible, have low manufacturing costs, and be semitransparent. These properties make them particularly advantageous for myriad of applications: e.g., use on non-planar surfaces, as tinted coatings on windows, any use for charging low power devices. One of the biggest problems preventing organic photovoltaics from being commercialized is controlling the packing of the organic materials within the active layer from the molecular scale through the mesoscale. The state-of-the-art method for preparing active layer offers essentially no control over packing through multiple length scales. In this dissertation, I present a method for controlling the active layer morphology from the molecular scale through the mesoscale using the assembly of organic nanoparticles.

The miniemulsion method was used to prepare nanosized particles of each of two active layer components, an electron donor and an electron acceptor. During

the nanoparticle synthesis, the internal molecular packing within the particles can be tuned by changing the "oil" (organic soluble) miniemulsion phase. The nanosized domains of each component were directly controlled by tuning the nanoparticle size during synthesis. This provides a large amount of control of the molecular scale packing and the nanoscale packing. Spray-coated assemblies of these nanoparticles, upon removing excess surfactant, were shown to transport charges with mobilities similar to those in films of pristine polymer made by standard drop-cast methods. Donor nanoparticles were mixed with acceptor nanoparticles and shown to form a random binary assembly of nanoparticles with charge conduction pathways. Organic photovoltaic devices were successfully prepared with a mixture of donor nanoparticles and acceptor nanoparticles, and gave performance comparable to analogous devices made by conventional film coating, bulk heterojunction methods. The internal morphology of the active layer films was shown to be easily tuned by changing the nanoparticle diameter or number ratio of donor nanoparticles to acceptor nanoparticles.

This method offers the ability to tune the molecular scale, nanoscale, or mesoscale, systematically, packing scales individually or collectively. Therefore, this method can be used to determine systematically what is the optimum active layer morphology for theoretically any donor plus acceptor combination of materials. Also, this method offers a way to control morphology and probe the properties of binary blends of organic materials, in a more general sense, e.g., for making other electronic devices or for charge mobility studies of solid films.

TABLE OF CONTENTS

Page

LIST OF TABLES

Table Page

LIST OF FIGURES

Figure Page

CHAPTER 1

INTRODUCTION: THE BROADER IMPACT POTENTIAL OF ORGANIC NANOPARTICLE PHOTOVOLTAICS AND ELECTRONICS

1.1 The Potential Industrial Impact of Organic Photovoltaics

In the growing global economy, organic electronic materials is a burgeoning market. A major IDTechEx report predicts that organic electronics will grow from a $29 billion market today to $73 billion by 2023.[1] This prediction includes organic light emitting diodes (OLED), organic photovoltaics (OPV), flexible electronic displays, organic transistors for logic and memory, sensors, and even batteries. The present market is predominantly OLEDs, although the report states the "huge growth potential" for the other sections of the market.

One of the largest areas of growth potential is the development of organic photovoltaics. The reason that they have so much potential is because they can open up new markets and be used in myriad untapped applications that conventional solar cells cannot access. The conventional market for solar cells is large power applications such as powering residential homes, and the leader in this market is silicon-based solar cells. Silicon cells are opaque, thick, heavy and rigid. Organic photovoltaics use carbon-based molecules, instead of silicon, and they are semi-transparent, thin, lightweight, and flexible. Simply put, they can be attached into anything, anywhere and in any size. This capability can open new markets and product avenues that are not possible with conventional silicon cells. Organic solar cells could achieve market breakthrough in two distinct and unconventional

markets: (1) outdoor use to absorb sunlight on non-planar surface, surfaces requiring a semitransparent film, and areas where silicon based photovoltaics are too heavy and (2) indoor use where they absorb the light emitted from indoor lighting such as LED. The possibilities are vast, from applications such as solar tinted windows, solar curtains, and solar umbrellas, to powering indoor devices such as calculators, toys and clocks. Thus organic photovoltaics can serve as a platform technology for myriad existing and new applications.

1.2 Organic Photovoltaics: Basic Introduction and Problems

Organic photovoltaics use organic molecules/polymers within a device active layer to convert sunlight into electricity. The active layer typically consists of two organic materials, an electron donor and an electron acceptor, depicted as orange and blue in Figure 1. The general mechanism for generating electricity using an organic photovoltaic starts with the absorption of photons in the active layer. Absorption of a photon excites an electron from a highest occupied molecular orbital (HOMO) level, or valence band level, to the lowest unoccupied molecular orbital (LUMO) level, or conduction band level, creating an exciton, an excited electron and hole pair. This exciton then must travel to the donor-acceptor interface otherwise it recombines and relaxes; at the interface, the electron can be donated an acceptor molecule, forming a charge-separated state. Then the electron has to travel through a continuous pathway of acceptor molecules to the cathode, and the hole (absence of an electron) has to travel through a continuous pathway of donor molecules to the anode. The collection of these charges at each electrode allows for

the flow of electrons generating electricity, and the charge transport needs to be balanced at each electrode to avoid power-inhibiting charge buildup. Each of these steps is intrinsically controlled by the packing of the donor and acceptor molecules/polymers at multiple length scales, from molecular-scale packing to continuous mesoscale structures. The resulting organic photovoltaic device performance is ultimately measured by its power conversion efficiency (PCE), which essentially is the percent of the photons' energy that is converted into electrical energy. The PCE is directly related to the efficiency of all of the steps described above. The efficiency of each step is closely related to the morphology of the active layer, thus the morphology directly impacts the PCE for all steps in the power conversion process.

What is the optimum morphology for the best PCE, or at least what do we know so far about this variable? The highest performing organic photovoltaic devices to date have an active layer morphology that is called the bulk heterojunction (BHJ). The BHJ morphology incorporates nanosized semicrystalline domains of the donor and the acceptor materials, packed with a large interfacial contact area and bicontinuous pathways to each electrode.[2,3] A cartoon describing this BHJ structure is shown in Figure 1.

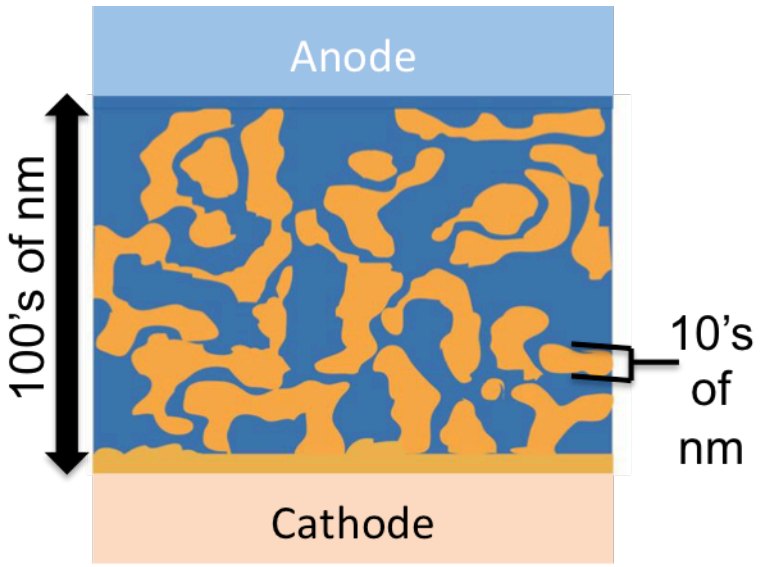

Figure 1: A Cartoon Depicting the Bulk Heterojunction Organic Photovoltaic Structure. Donor and Acceptor Materials are Depicted as Blue and Orange Here, Respectively. Scale Bars Included to Demonstrate Mesoscale and Nanoscale Domains.

To date, the prototypical materials used to form and exemplify the BHJ structure are regioregular poly(3-hexylthiophene) (P3HT, the donor) and phenyl-C_{61}-butyric acid methyl ester ($PC_{61}BM$, the acceptor). P3HT and $PC_{61}BM$ is one of the best known systems that form a BHJ morphology, and numerous studies have been performed to elucidate the BHJ features.[2,4-7] It was determined that to form this BHJ morphology, (1) P3HT has to be able to crystalize in the presence of $PC_{61}BM$, (2) $PC_{61}BM$ has to be able to easily diffuse through amorphous P3HT, and (3) $PC_{61}BM$ must then slowly crystalize in the presence of P3HT. P3HT and $PC_{61}BM$ were shown using HR-TEM and AFM to form interspersed nanoscale phase domains with sizes around 10 nm – 15nm, as seen in Figure 2.[5,8] Initial reports – and still widely accepted – estimates for the exciton diffusion length in P3HT is 5 nm – 10 nm,[9] which correlates well with why optimum domain sizes of 10 nm – 15 nm in the P3HT/PCBM solar cells would work well. The basic premise is that the electron-hole

pair can only travel about that far before recombining, so large size scales should detract from performance. Therefore, as the typical discussion goes, a well-optimized BHJ morphology, as for the P3HT and $PC_{61}BM$ example, has phase separated regions of 10 nm – 15 nm scale with semicrystalline donor and acceptor regions giving well-interspersed pathways to each electrode.

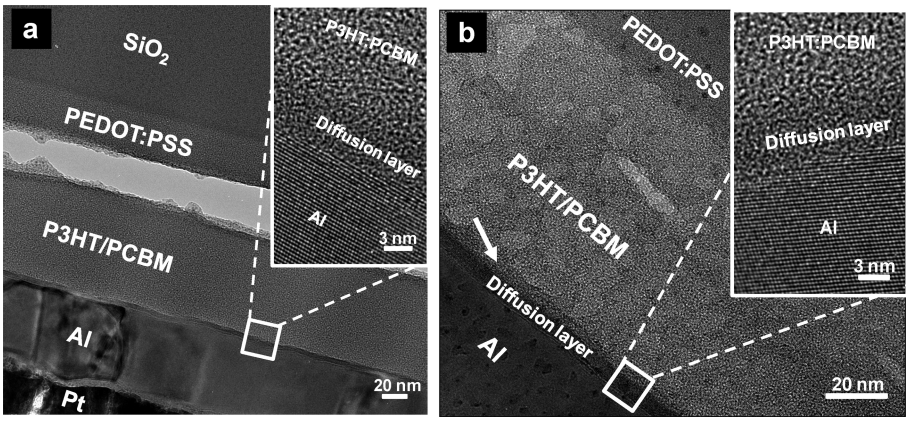

Figure 2: a) HR-TEM Image of a Cross Sectioned P3HT/PCBM BHJ Device Before Annealing, b) and After Annealing. Reprinted with Permission from Chen, D. A.; Nakahara, A.; Wei, D. G.; Nordlund, D.; Russell, T. P. P3HT/PCBM Bulk Heterojunction Organic Photovoltaics: Correlating Efficiency and Morphology. *Nano Lett.* 2011, 11, 561. Copyright 2011 American Chemical Society.

The BHJ structure of P3HT and PCBM is formed by thermally annealing the mixture of components in the solid-state device. It was discovered that other lower band gap polymers can also form BHJ structures, with the assistance of active layer processing additives. One of the first low band gap systems shown to do this was poly(2,6-(4,4-bis(2-ethylhexyl)-4H-cyclopenta[2,1-b;3,4-b′]-dithiophene)-*alt*-4,7-(2,1,3-benzothiadiazole)) (PCPDTBT) with $PC_{71}BM$.[10,11] It was shown that the additives, typically 1,8-diiodooctane, selectively solubilize the $PC_{71}BM$ allowing it to diffuse out of a PCPDTBT-rich phase, allowing PCPDTBT to crystalize and $PC_{71}BM$ to crystalize slowly into nanosized aggregates. The Russell group at UMass Amherst

investigated the morphology of this system further using X-ray scattering, neutron scattering, X-ray diffraction, and transmission electron microscopy (TEM).[12] They found that, when an additive was used, a hierarchical morphology of PCPDTBT fibrils forms in a matrix of amorphous PCPDTBT and $PC_{71}BM$, as shown in Figure 3. Russell's results are consistent with what Bazan and coworkers proposed, that the additive preferentially solubilizes $PC_{71}BM$ *not* PCPDTBT, allowing $PC_{71}BM$ to diffuse through PCPDTBT, and thus allowing PCPDTBT to form fibril crystallites of nanosized thickness. Using grazing incidence small angle X-ray scattering (GISAXS), grazing incidence wide angle X-ray scattering (GIWAXS), TEM, and Kelvin probe force microscopy, Su and coworkers determined that PCPDTBT and $PC_{71}BM$ actually form a bi-hierarchical nanostructured morphology.[13] They propose that the fibril-like PCPDTBT structures are actually small spherical-like crystallites of PCPDTBT packed together to form large structures on the order of 100 nm, as shown in Figure 4. As these spherical PCPDTBT crystallites form and pack together, $PC_{71}BM$ is forced out of the phase, forming $PC_{71}BM$ clusters with regions of amorphous PCPDTBT mixed with $PC_{71}BM$.

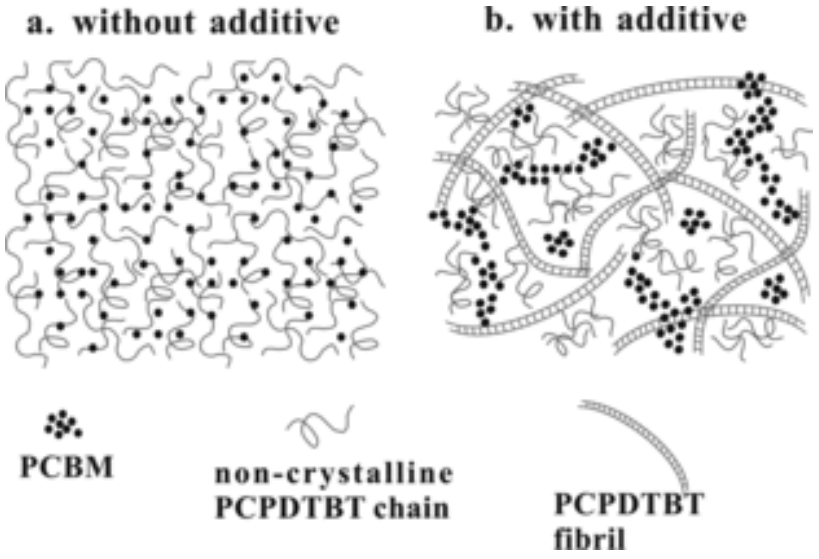

Figure 3: Cartoon Describing PCPDTBT:PCBM Morphology a) Without an Additive, and b) With an Additive (e.g., 1,8-diiodooctante). Adapted with Permission from Gu, Y.; Wang, C.; Russell, T. P. Multi-Length-Scale Morphologies in PCPDTBT/PCBM Bulk-Heterojunction Solar Cells. *Adv. Energy Mater.* 2012, 2, 683. Copyright (c) 2012 WILEY-VCH Verlag GmbH & Co. KGaA, Weinheim. http://onlinelibrary.wiley.com.silk.library.umass.edu/doi/10.1002/aenm.201100726/full

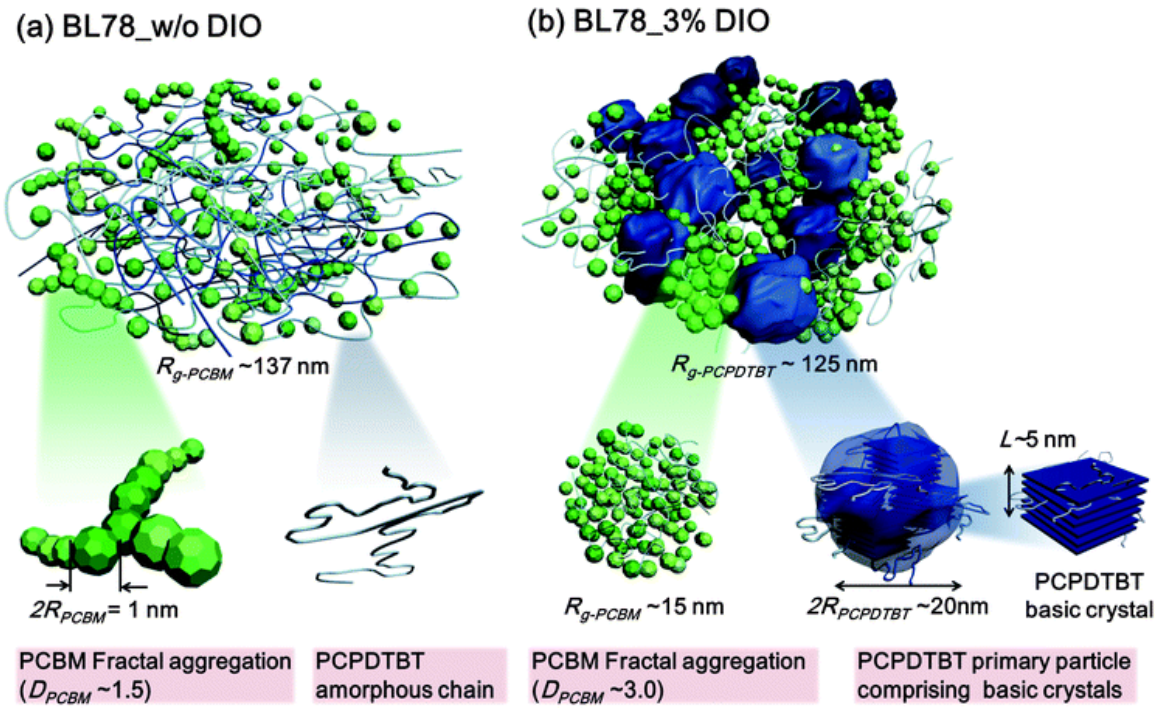

Figure 4: Cartoon Showing PCPDTBT BHJ Morphology a) Without Additive, and b) With Additive. Reproduced from Liao, H. C.; Tsao, C. S.; Shao, Y. T.; Chang, S. Y.; Huang, Y. C.; Chuang, C. M.; Lin, T. H.; Chen, C. Y.; Su, C. J.; Jeng, U. S.; Chen, Y. F.; Su, W. F. Bi-hierarchical Nanostructures of Donor-Acceptor Copolymer and Fullerene for High Efficient Bulk Heterojunction Solar Cells. *Energy Environ. Sci.* 2013, 6, 1938. with Permission of The Royal Society of Chemistry.

Trying to understand the BHJ morphology and the optimal morphology for organic photovoltaics, Darling and coworkers thoroughly investigated the morphology of PTB7/$PC_{61}BM$ device structures.[14] PTB7 with PCBM is one of the highest performing single active layer organic photovoltaic device formulations, with PCEs ranging from 7-9%. Using X-ray scattering techniques, X-ray reflectivity, TEM, and tuning of the active layer crystallinity and degree of phase separation by changing the initial fabrication solvent, Darling and coworkers developed the detailed picture of an optimized BHJ morphology shown in Figure 5. They found that PTB7 and $PC_{61}BM$ does form a hierarchical morphology that includes nanosized

aggregates of PTB7 and $PC_{61}BM$, but also forms PTB7-rich and $PC_{61}BM$-rich domains on the scale of hundreds of nanometers. Darling and coworkers highlight in this work that this device architecture benefits from *not* having discrete interfaces between PTB7 and $PC_{61}BM$. They state that PTB7 crystallites benefit from having intermixed PTB7 and $PC_{61}BM$ surrounding them to allow for efficient electron transfer, because the charges are better stabilized in the intermixed region. PTB7 crystallites in large PTB7 rich domains (hundreds of nanometers in size) help exciton dissociation because of the high charge mobility within the crystallites, providing a charge carrier "highway" to allow easier hole hopping through the PTB7-rich domain to an electrode, while electrons separate to the $PC_{61}BM$-rich domain to hop to the other electrode.

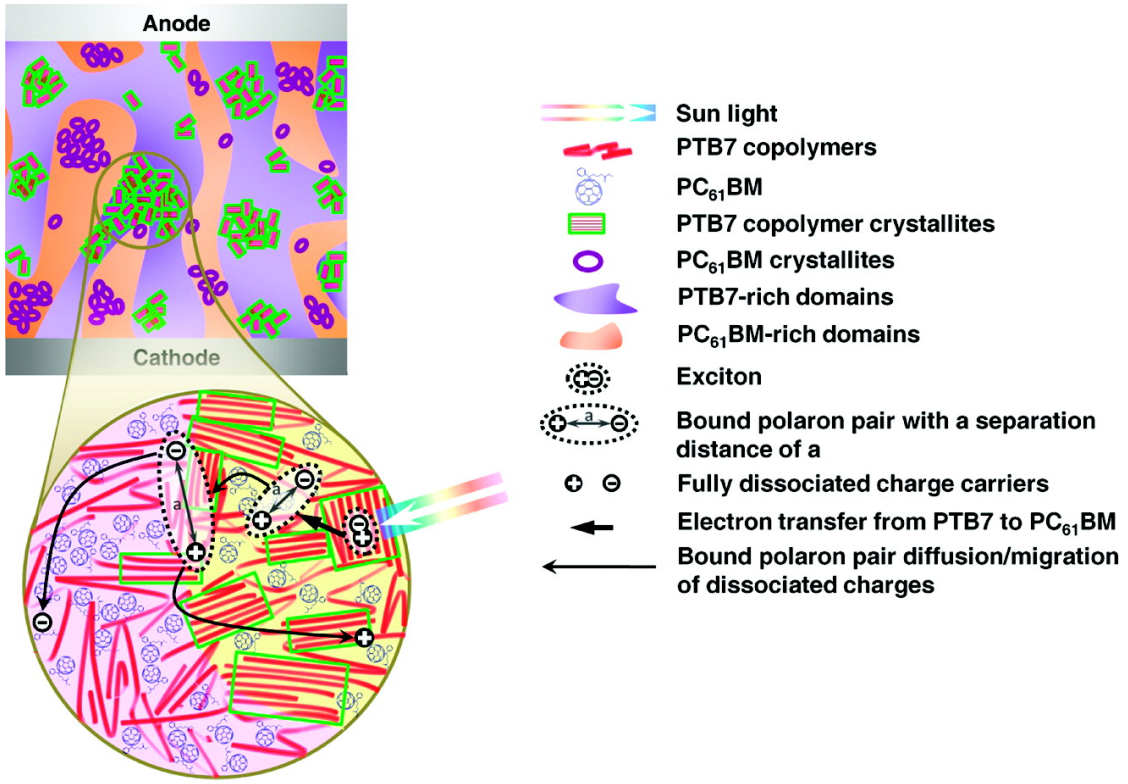

Figure 5: Darling and Coworkers' Model Describing the PTB7 and $PC_{61}BM$ Active Layer Morphology. Reprinted with Permission from Chen, W.; Xu, T.; He, F.; Wang, W.; Wang, C.; Strzalka, J.; Liu, Y.; Wen, J. G.; Miller, D. J.; Chen, J. H.; Hong, K. L.; Yu, L. P.; Darling, S. B. Hierarchical Nanomorphologies Promote Exciton Dissociation in Polymer/Fullerene Bulk Heterojunction Solar Cells. *Nano Lett.* 2011, 11, 3707. Copyright 2011 American Chemical Society.

Using PTB7 and switching from $PC_{61}BM$ to $PC_{71}BM$ in a BHJ solar cell results in improved PCE values up to 9.2%.[15] But, Samuel and coworkers[16] found that this mixture formed a different morphology than what Darling and coworkers described. First they found that without using the additive DIO, large domains hundreds of nm long were formed, that were not actually pure $PC_{71}BM$ but instead fullerene rich domains, with smaller spherical pure fullerene domains 20 – 60 nm in size, surrounded by a PTB7 matrix within the large $PC_{71}BM$ rich domain. Then when the DIO additive is used, fibril like structures of PTB7 and $PC_{71}BM$ form with

thicknesses of tens of nm and lengths on the scale of hundreds of nm. Photoconductive atomic force microscopy (pc-afm) results indicate that there is a concentration gradient of donor and acceptor between the PTB7-rich domains and $PC_{71}BM$-rich domains, which aids in exciton diffusion. The device internal quantum efficiency (IQE) jumps from 40%-60% to 80%-90% when using the DIO additive, which the authors attribute to the formation of the fibril-like domains as aids in charge extraction. This is because upon charge separation the free charges are readily transported through the fibril-like domain "highways" where recombination is minimal.

The view of the "optimum" morphology for organic photovoltaics has evolved extensively throughout the past 10 years, despite (or perhaps because of) the difficulties to probe the assembly from the molecular scale through the mesoscale. The initial view of the BHJ morphology was the two-phase picture with separated nanosized domains of the donor and the acceptor. The work by Samuel and coworkers suggests a need for a three-phase system: (1) donor-rich fibril regions with a width on the order of tens of nm and length on the order of hundreds of nms; (2) similar acceptor fibril regions; (3) between the donor and acceptor fibrils, a third phase of intermixed donor and acceptor that facilitates exciton transport. But, even know, although much has been learned about what might be needed for the "optimum" morphology in organic photovoltaics, there is no method to tune the morphology easily and systematically to test this. My work is aimed at attempting to address this problem.

1.3 Systematically Forming the Optimum Organic Photovoltaic Morphology

The state-of-the-art method to prepare an active layer in organic photovoltaics consists of mixing an electron donor (typically a polymer) with an electron acceptor (typically a fullerene based molecule) in a common solvent (typically xylene, chloroform, chlorobenzene, or *o*-dichlorobenzene). This solution is thoroughly mixed and then spin-coated on top of an interlayer coated electrode, hoping that the BHJ structure is formed. If the BHJ structure is not formed, the films are annealed at a variety of temperatures for a range of times in hopes to form the BHJ structure. If this does not work then a wide range of additives[17] can be added to the initial solvent mixture, in hopes to solubilize one of the components preferentially and form the BHJ structure. There have been many donating and accepting polymers and molecules synthesized that absorb a lot of the solar spectrum, ideally to be used in organic photovoltaic devices. But, only a small fraction of these polymers/molecules form the BHJ structure described above, and if they do not form this structure they are not very efficient for present solar cell fabrication techniques. Therefore, it is greatly desired to be able to tune the morphology systematically, and develop a method to form a BHJ-like morphology on demand with any donor-acceptor pairing of choice. In a 2015 perspective titled "The Next Breakthrough for Organic Photovoltaics?", Mark Ratner, Tobin Marks and coworkers end their paper with, "We reiterate that future OPV efficiency gains will likely come not from completely empirical combinatorial synthesis of new materials with optimum energy levels but from novel design criteria that include but go beyond energy levels *allowing for the development of systematic understanding-*

based protocols to control the active layer morphology and perfect processing techniques."[18]

1.4 Organic Nanoparticles for a Systematically Assembled Morphology in Organic Photovoltaics

It would be greatly desirable to develop a method where one could form a BHJ-like morphology reliably with any donor-acceptor combination. In an attempt to do this, D. Venkataraman (DV Group) developed a strategy to control the morphology and packing all the way from the molecular scale (typically 0.1 nm – 1.0 nm) through the mesoscale (typically 150 nm – 1000 nm), based on nanoparticle pre-assembly and BHJ formation by size-based particle assembly. As seen in Figure 6, the donor and acceptor (shown as P3HT and PCBM) can each be prepared as spherical nanoparticles. As part of the nanoparticle synthesis the internal molecular or polymer chain packing can be tuned.[19] The nanoparticle diameter can also tuned, which is extremely advantageous because nanosize domain control is required for efficient organic photovoltaic device operation. Finally, donor and acceptor nanoparticles can be combined in solution and prepared as films, forming a mesoscale co-mingled assembly of donor and acceptor particles. Fundamental geometric assembly of spheres directs the formation of the mesoscale assemblies, instead of relying on a delicate balance of intermolecular interactions between donating and accepting molecules or polymers (the current methodology). Controlling and tuning the morphology of organic photovoltaics is extremely challenging, and indeed random, with the current method for preparing the active layer. The organic nanoparticle method allows for systematic control of the active

layer morphology at all scales of assembly from molecular packing through the mesoscale packing of the active layer.

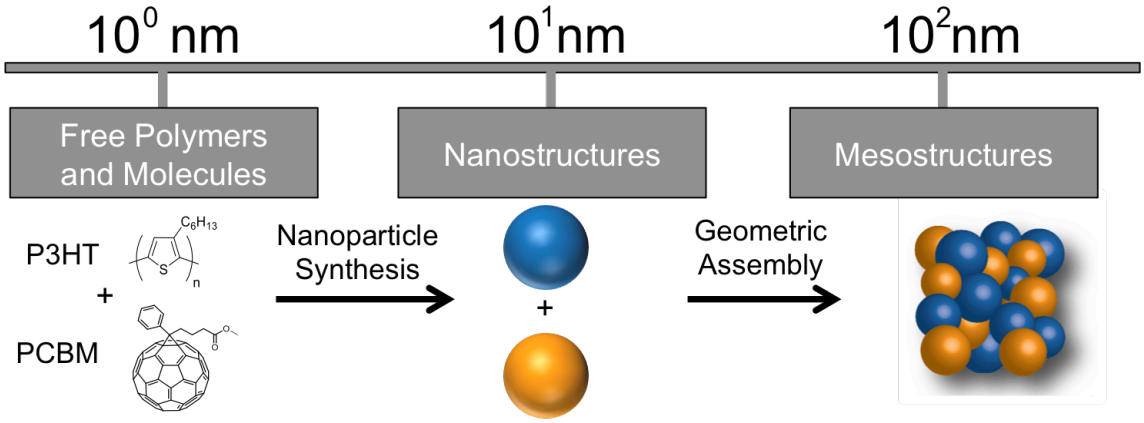

Figure 6: Organic Nanoparticle Method to Tune the Morphology from the Molecular Scale Through the Mesoscale

When the nanoparticles assemble on a substrate, they can form ordered assemblies of binary nanoparticle superlattices or a random binary assembly, as shown in Figure 7. Ordered binary nanoparticle superlattices have been prepared using organic nanoparticles[20,21] and inorganic nanoparticles[22,23]. The packing within these ordered structures can be tuned by changing the radius ratio of the two types of nanoparticles. This is advantageous for use in organic nanoparticle photovoltaics, allowing one to tune the binary superlattice structure systematically to vary the interfacial contact area between donating and accepting nanoparticles, as well as to tune the formation of charge transport percolation pathways for each particle type.

One of the main disadvantages for using *ordered* nanoparticle superlattices for organic photovoltaics is that they have only been prepared on very small scales (square micrometers). Therefore, it would be very difficult to transfer this methodology to a commercial scale. By comparison, random nanoparticle

assemblies can be prepared over large areas, as my work demonstrated. As seen in Figure 7, random nanoparticle assemblies still form percolation pathways for each type of particle, with large interfacial contact areas. Lawrence Renna in the DV group is showing how the nanoparticle packing in random binary nanoparticle assemblies can be directly assessed, using conducting atomic force microscopy paired with simulations. The packing within binary nanoparticle assemblies can be systematically tuned by changing the radius ratio and relative concentrations between the two types of nanoparticles. The abilities to prepare large area assemblies and to tune packing within random binary nanoparticle assemblies, makes them very attractive for use in organic photovoltaics and similarly-fabricated electronic devices.

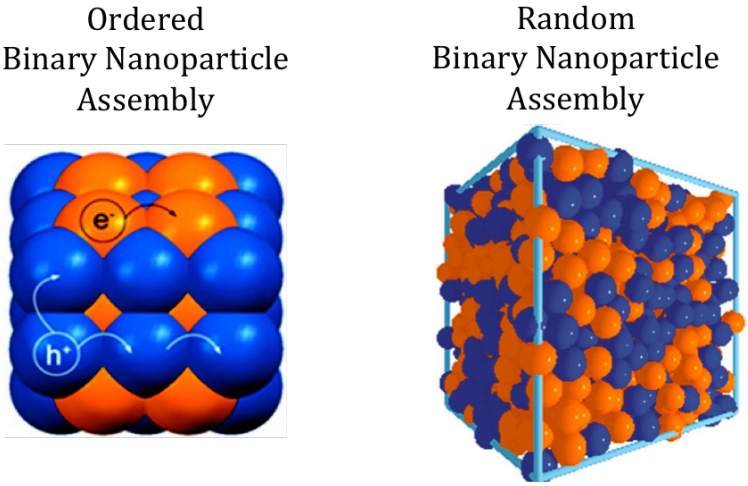

Figure 7: Ordered Binary Nanoparticle Assembly vs. Random Binary Nanoparticle Assembly

It would be extremely disruptive to the field of organic photovoltaics, if a method were devised such that the active layer morphology could be systematically tuned. This would greatly speed the determination of the optimal morphology for

both old and new component mixtures being considered for organic photovoltaics. Using the organic nanoparticle based method; one could in principle easily tune morphology for any mixture of active layer materials. Therefore, one could then readily determine whether "optimum" morphological features are universal for donating and accepting materials, or whether they are material dependent properties. The latter situation is entirely possible, since various conjugated polymers/molecules have a wide range of electrical properties (e.g., charge mobility).

For the nanoparticle methodology to be successful, several things have to be proven. First, the nanoparticle synthesis step has to be very versatile and applicable to a wide range of active layer materials. The synthesis has to allow for internal structure (molecule or polymer chain packing) of the nanoparticles to be tuned. Also, the size and dispersity of the nanoparticles has to be easily controlled and tuned. Then, the nanoparticles must be compatible with assembly in a way that will not impede charge transfer/transport through the nanoparticle-based phase. Following what has been learned from the works of Darling and Samuel, it may be important to create an intermixed region between nanoparticles to help with efficient exciton diffusion. Finally, the nanoparticle assemblies need to be prepared in a manner that is compatible with organic photovoltaic architecture.

In the following sections of this dissertation, I will describe how I used the prototypical active layer materials P3HT and PCBM to develop the nanoparticle random assembly method to address all the issues described above, including the preparation of organic nanoparticle photovoltaic devices. Chapter 2 starts with the

optimization of the miniemulsion nanoparticle synthesis method to reproducibly prepare nanoparticles with tunable size and internal structure. Allowing for direct control of the molecular packing and the nanosized domains. Chapter 3 discusses the assembly of these nanoparticles and determines whether the electrically insulating surfactants impede charge transport. Chapter 4 describes the preparation of binary nanoparticle assemblies of P3HT nanoparticles and PCBM nanoparticles. It clearly shows the formation of a random binary assembly of nanoparticles. Chapter 4 also demonstrates organic photovoltaic devices can be prepared using a binary nanoparticle assembly as the active layer with tunable morphology. Chapter 5 discusses the immediate impact of this work and future directions. Chapter 6 discusses in detail the experimental methods used.

CHAPTER 2

NANOPARTICLE SYNTHESIS OF CONJUGATED ORGANIC POLYMERS AND MOLECULES

2.1 Introduction to Conjugated Polymer/Molecule Nanoparticle Synthesis

Adapted with permissions from Renna, L. A.; Gehan, T. S.; Venkataraman, D. In Optical Properties of Functional Polymers and Nano Engineering Applications; Jain, V., Kokil, A., Eds.; CRC Press: Boca Raton, FL USA, 2014; Vol. 1, pp 227-252.

Conjugated polymer nanoparticles have been shown to be very useful materials for a wide variety of applications including optoelectronic devices,[24-28] biological sensing/imaging,[29-33] and gene/drug delivery.[29,34] There are two common methods for synthesizing conjugated polymer nanoparticles: the reprecipitation method and the miniemulsion method.[32,35,36] In the reprecipitation method the desired polymer is dissolved in a "good" solvent (e.g., tetrahydrofuran (THF)), and then added into a "bad" solvent (e.g., water) for the polymer, while vigorously stirring or sonicating. In the miniemulsion method a polymer or a monomer is dissolved in the organic ("oil") phase, which is then added to a water phase containing a surfactant. The mixture is sonicated and then the solvent is either evaporated or the monomer is polymerized to form the nanoparticle dispersion.

One main advantage that the miniemulsion method has over the reprecipitation method is that one can start either from presynthesized polymers (post polymerization nanoparticle synthesis) or from monomers and then synthesize the polymer within the emulsion droplets (direct polymerization nanoparticle synthesis). Both methods have been used to prepare nanoparticles

with a wide range of sizes from 10s of nm – 100s of nm.[35] Typically a small concentration of polymer has to be used with the reprecipitation method. Since high concentrations of polymer in solution are needed to prepare organic photovoltaic devices, the rest of the DV group and myself chose to use the miniemulsion method.

For a typical miniemulsion preparation the desired polymer is dissolved in an organic solvent that is not miscible with water (e.g., chloroform, toluene, xylene, chlorobenzene) and injected into an aqueous solution containing surfactants (e.g., sodium dodecyl sulfate, cetyltrimethylammonium bromide, Triton X-100). The biphasic mixture is stirred for about an hour to form a macroemulsion, where the organic solvent droplets are larger than 1 μm. Then an ultrasonicator is used to break up the macroemulsion droplets, forming a miniemulsion of smaller droplets with sizes ranging from 30 nm – 500 nm.[37] These droplets are claimed to be monodisperse and stabilized by the surfactant in solution, with the droplet size dependent on multiple variables: surfactant concentration, organic solvent to water volume ratio, organic solvent used,[38] and sonication power.[39] To our knowledge, the effect each of these variables has on conjugated nanoparticles properties has not been fully explored to date, and the extent is not fully known to which each parameter affects the nanoparticle internal structure and size. Coalescence of droplets can occur due to Ostwald ripening, where the organic solvent diffuses from the droplet. Ostwald ripening can be prevented by using an ultrahydrophobe, typically a long linear hydrocarbon or even a portion of the polymer itself in solution. After forming the miniemulsion the solution is stirred and heated to remove the organic solvent, forcing the polymers in solution to aggregate, leaving a

surfactant stabilized conjugated polymer nanoparticle dispersion as shown in Figure 8[24].

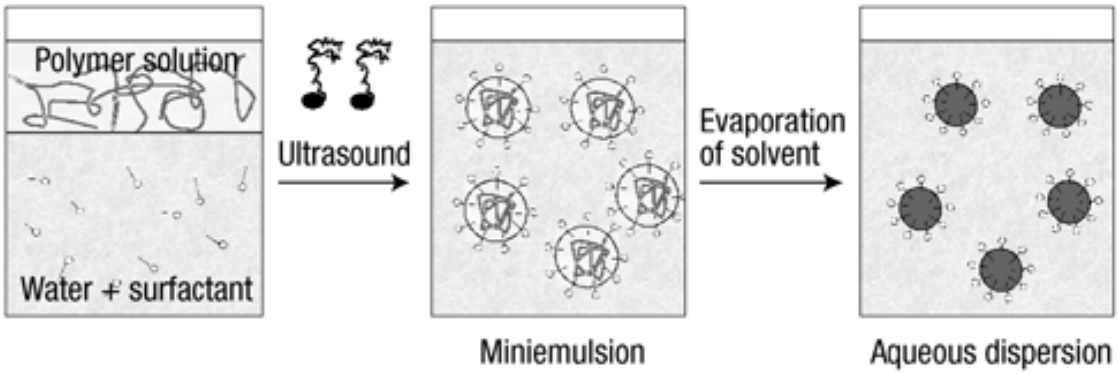

Figure 8: Cartoon Depicting the Generalized Miniemulsion Method for Preparing Polymer Nanoparticles. Reprinted by Permission from Macmillan Publishers Ltd: Nature Materials. Kietzke, T.; Neher, D.; Landfester, K.; Montenegro, R.; Guntner, R.; Scherf, U. Novel Approaches to Polymer Blends Based on Polymer Nanoparticles. Nat. Mater. 2003, 2, 408., copyright 2003.

Ionic small molecule surfactants are typically used to stabilize and achieve nanometer-sized droplets. Polymeric surfactants have also been used but are not as common, especially for conjugated polymer nanoparticles.[40] Sodium dodecyl sulfate (SDS) is the most common surfactant used for synthesizing conjugated polymer nanoparticles. Antonietti and co-workers have shown that cationic surfactants such as cetyltrimethylammonium bromide (CTAB) can also be used as the surfactant.[41]

2.2 Ultrasonication for Miniemulsion Nanoparticle Synthesis

When using probe tip ultrasonication to prepare a miniemulsion, the main goal for efficient sonication is to have uniform and effective cavitation within the solution. Cavitation is when sonic waves propagate through a solution, creating bubbles that grow larger until they finally collapse on themselves.[42,43] Cavitation occurs when "the ultrasonic pressure exceeds the average pressure in a liquid, the

pressure of the latter falls below zero, and the medium fragments into small cavities which expand as the pressure rises and then, as the pressure starts to fall, become unstable and collapse violently."[44] The collapsing of these bubbles creates local shear forces in solution, which break up the emulsion droplets into smaller droplets. There are many variables that can affect the cavitation process including: sonication frequency, sonication intensity, solvent properties (e.g., vapor pressure, viscosity, surface tension), temperature, and the external pressure.[45] For efficient sonication, "dead-zones" must be minimized within the solution. Dead-zone areas have inefficient cavitation, and can be caused by inefficient circulation of the solution, improper tip size to vessel size, and even the sonication vessel shape. Figure 9 shows six different vessel shapes that were tested to determine which shape gave the most efficient sonication.[46] From this study it was found that vessels A-C all promote efficient sonication.

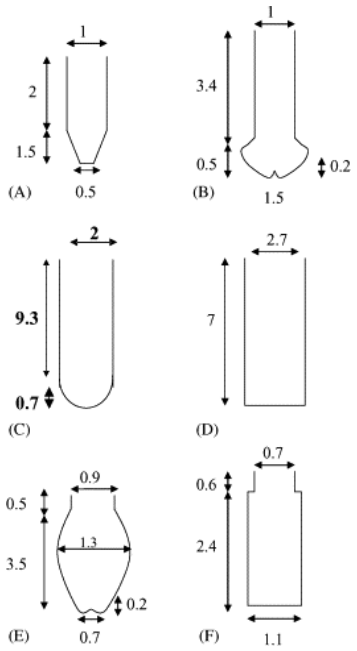

Figure 9: Various Vessel Shapes Used for Ultrasonication. Vessels A-C Minimize Sonication Dead Zones Most Efficiently. Reprinted from Talanta, Vol 66/Issue 5, Capelo, J. L.; Galesio, M. M.; Felisberto, G. M.; Vaz, C.; Pessoa, J. C., Micro-Focused Ultrasonic Solid-Liquid Extraction (μFUSLE) Combined with HPLC and Fluorescence Detection for PAHs Determination in Sediments: Optimization and Linking with the Analytical Minimalism Concept., 1272-1280, Copyright 2005, with permission from Elsevier.

2.3 The Evolution and Optimization of the Miniemulsion Nanoparticle Synthetic Method Used by the Venkataraman Group

Before I joined the DV group, they were already preparing conjugated polymer nanoparticles using the miniemulsion method with a bath sonicator to induce cavitation within the solution. The problem with using a bath sonicator is that the sonication intensity varies substantially at different areas within the bath. Therefore, the size of the produced nanoparticles will change depending on where the vial is held within the bath, making it difficult to reproduce the results. Therefore, the group decided to switch to using a probe tip sonicator in attempt to

prepare conjugated polymer nanoparticles with reproducible size, as this method was expected to give more reproducible caviation within solution.

The previously established procedure for the DV group to prepare conjugated polymer nanoparticles was established by Dana Algaier, G. Nagarjuna, and B. Harihara Venkatraman. As the long-term goal was to prepare organic photovoltaic devices, the initial optimization of nanoparticle synthesis was done using P3HT as the conjugated polymer, since it is an archetypical hole transporting material. The surfactant used was sodium dodecyl sulfate (SDS), because it was in very common use in miniemulsion procedures. The goal of optimizing the nanoparticle synthetic procedure is to prepare the smallest possible nanoparticles, because if the heterogeneous solution formulation were held constant (volume ratio of oil:water, constant concentrations of P3HT and surfactant) then the smallest nanoparticles would indicate the most efficient sonication / cavitation. Because organic polymer exciton diffusion length was estimated to be ~10 nm during the time of that work, a successful desired outcome was to prepare nanoparticles as small as 20 nm. During the original optimization previous group members prepared emulsions of a P3HT chloroform solution mixed with a SDS in water solution, an "oil-in-water emulsion". They then used a 20mL cylindrical vial as the sonication vessel, they optimized the sonication conditions: sonication power and sonication time with a 1/8" titanium probe tip. They also investigated the effect that polymer concentration, surfactant concentration, and the volume ratio of polymer solution to surfactant had on the average nanoparticle diameter. The average nanoparticle diameter was determined using dynamic light scattering (DLS). Based on the best

optimized procedure using their optimized procedure with a probe tip sonicator, P3HT nanoparticles could be prepared reproducibly with predictable size that can be tuned by changing the polymer or surfactant concentration.

After learning this optimized procedure, I performed an experiment that did not seem consistent with reports in the literature. Using the established method to prepare P3HT nanoparticles from a 5 mg/mL solution of P3HT in chloroform mixed with a 1 mM SDS in water solution resulted in P3HT nanoparticles with an average diameter of ~140 nm, based on DLS. But, when using the same concentration of polymer solution but with a 1mM cetyltrimethylammonium bromide (CTAB) solution, a positively charged surfactant, the average nanoparticle diameter was ~90 nm. Landfester and coworkers, Landfester and Antonietti are very well known in the field of miniemulsion nanoparticle synthesis, reported that using the same concentration of SDS and CTAB resulted in nanoparticles with similar average diameters (using polystyrene).[41] When using 10 mM surfactant they obtained 138 nm and 120 nm respectively, and when 20 mM surfactant was used they obtained 93 nm and 89 nm nanoparticles respectively. This was done by miniemulsion polymerization of monomers, but it still suggested that using SDS and CTAB at the same concentrations it should give similarly-sized droplets within the emulsion.

In our miniemulsion method, we assumed the rate of evaporation of chloroform to be relatively constant whether SDS or CTAB is used since they are heated at the same temperature above the chloroform boiling point. Therefore, something appeared to be different in how our procedure was working, since we

have drastically different P3HT nanoparticle sizes when using SDS (138 nm) and CTAB (90 nm).

Most of the literature on the nanoparticle synthesis using the miniemulsion method is imprecise about specific sonication parameters used to prepare the miniemulsions. Looking further into the sonochemistry literature, I found that a cylindrical, flat-bottom vial might not be the most effective vessel shape for efficient sonication, as described in Figure 9. Therefore, I switched the procedure from using a cylindrical vial to a conical tube that tapered down to the bottom. For the typical total volume of our procedure, 3.3 mL to 3.5 mL, a 15 mL conical centrifuge tube was appropriate to contain the solution during sonication. Using centrifuge tubes also allows for the tubes to be easily cooled in an ice bath during sonication. The probe tip heats up during continuous sonication, and cavitation is more efficient when the solution is cooled.

Upon switching to a cooled centrifuge tube for sonication, I prepared the same P3HT solutions described above for the established method: 5 mg/mL of P3HT solution in chloroform mixed with 1 mM SDS solution in a cooled centrifuge tube yielded ~80 nm P3HT nanoparticles. Using the same solutions and conditions, except for switching from 1 mM SDS to 1 mM CTAB, also yielded in ~80 nm P3HT nanoparticles. These results indicate that using a centrifuge tube allows for more efficient sonication and higher confidence in reproducibility, because it minimizes dead zones and allows better circulation of the emulsion solution during sonication. Please see the experimental section in chapter 6 for more specific details of the nanoparticle synthesis procedure.

The recent literature expectation is that as the surfactant concentration increases, the nanoparticle diameter decreases, although, this is only taken as a generalization, and the extent upon which the many possible variables might be related is not well understood. To understand in further detail the effect of the sonication vessel on the nanoparticle diameter, fifteen nanoparticle solutions were prepared with five different concentrations of surfactant solution (1.0, 2.5, 5.0, 10, and 20 or 25 mM SDS) and three different concentrations of polystyrene solution (1,10, and 30 mg/mL). Both cylindrical vials (labeled Vial) and conical centrifuge tubes (labeled CT) were used, as shown in Figure 10. A constant volume ratio (1:10) of polymer solution to surfactant solution was used for each sample. DLS was used to measure the resulting average nanoparticle diameters. When using a cylindrical vial, at 1 mg/mL polystyrene, as the concentration of surfactant increased the nanoparticle diameter decreased. But, as the concentration of polymer increased (10 mg/mL and 30 mg/mL) the nanoparticle diameter became less affected by surfactant concentration, which is not consistent with literature reports. But after switching to a centrifuge tube to prepare the miniemulsion, for all three concentrations of polymer solution, as the surfactant concentration increases the average nanoparticle diameter decreases, which is consistent with the literature. Therefore, these results paired with the results comparing SDS and CTAB nanoparticles, indicate that using a centrifuge tube allows for more efficient sonication to prepare smaller diameter conjugated polymer nanoparticles when using ultrasonicator probe tips to prepare miniemulsions.

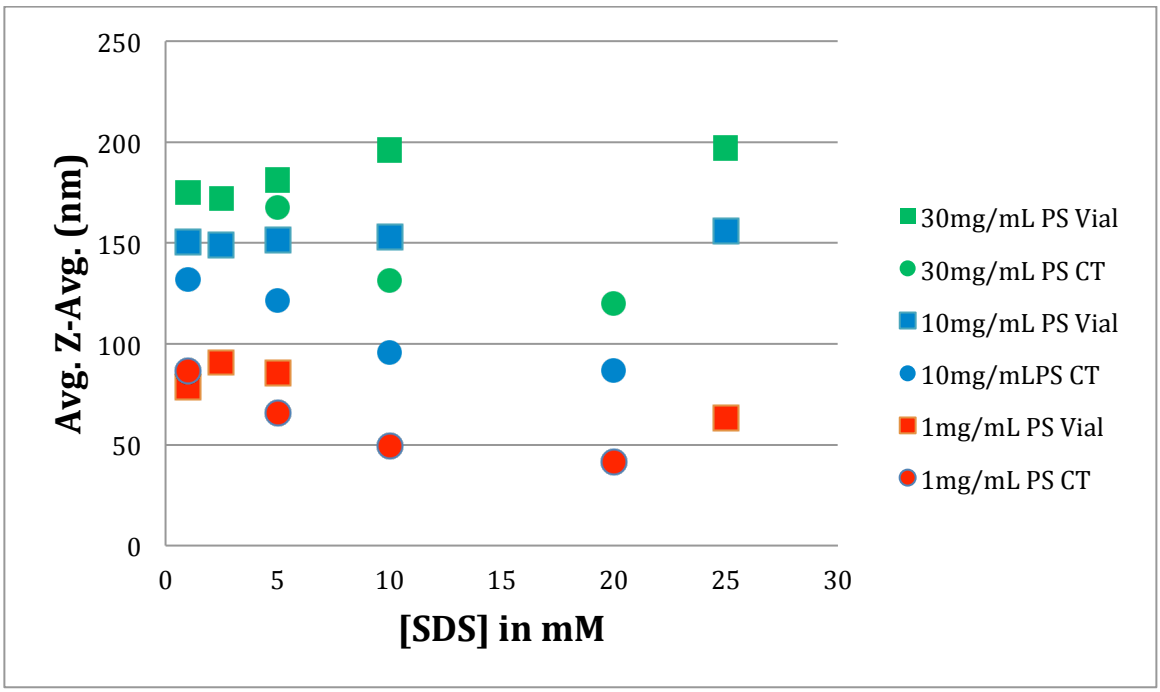

Figure 10: Comparing Nanoparticle Average Diameter Using a Centrifuge Tube and a Cylindrical Vial During the Sonication Process Using the Miniemulsion Method.

2.4 Nanoparticle Average Diameter and Diameter Dispersity Control

As discussed previously, in the miniemulsion method, it is known that the average polymer nanoparticle size decreases as the surfactant concentration increases and polymer concentration decreases. An important part of my work was to confirm the degree with which this applied to the modified mini-emulsion procedures that I was developing. Another was to try to gain more detailed data about the nanoparticle diameters and the dispersity of diameters produced by the procedure. This required extensive use of methodology that only recently has become more common in such work.

The average nanoparticle diameter is typically measured by dynamic light scattering (DLS). Other methods typically used to measure average nanoparticle

diameters are: transmission electron microscopy (TEM), scanning electron microscopy (SEM), atomic force microscopy (AFM), and photon correlation spectroscopy (PCS). DLS is convenient because it is one of the few solution-based measurement methods, having relatively short sample preparation/measurement times to yield properties for the bulk of the sample. Although DLS is good for determining the average nanoparticle diameters, it does not accurately determine the nanoparticle size distribution, specifically for polydisperse nanoparticle samples.[47] One of the newer techniques for determining the average nanoparticle diameter is Nanoparticle Tracking Analysis (NTA). A major benefit of NTA is that it tracks and evaluates individual nanoparticles in solution; therefore, it can accurately yield nanoparticle diameter distribution for a bulk sample. For similar reasons, NTA is one of the few techniques to be able to also measure the *concentration* of nanoparticles in solution. NTA therefore can give a mode diameter, the diameter exhibited by the highest number of nanoparticles: it will also determine the standard deviation of the nanoparticle diameter distribution.

Figure 11 demonstrates how the mode diameter for P3HT nanoparticles made by the mini-emulsion method, as determined by NTA, changes with surfactant concentration. As the concentration of surfactant increases the nanoparticle diameter decreases. I found that, typically, if one increased the polymer concentration, then the whole curve of Figure 11 shifts up: decreased polymer concentration shifts the whole curve down.

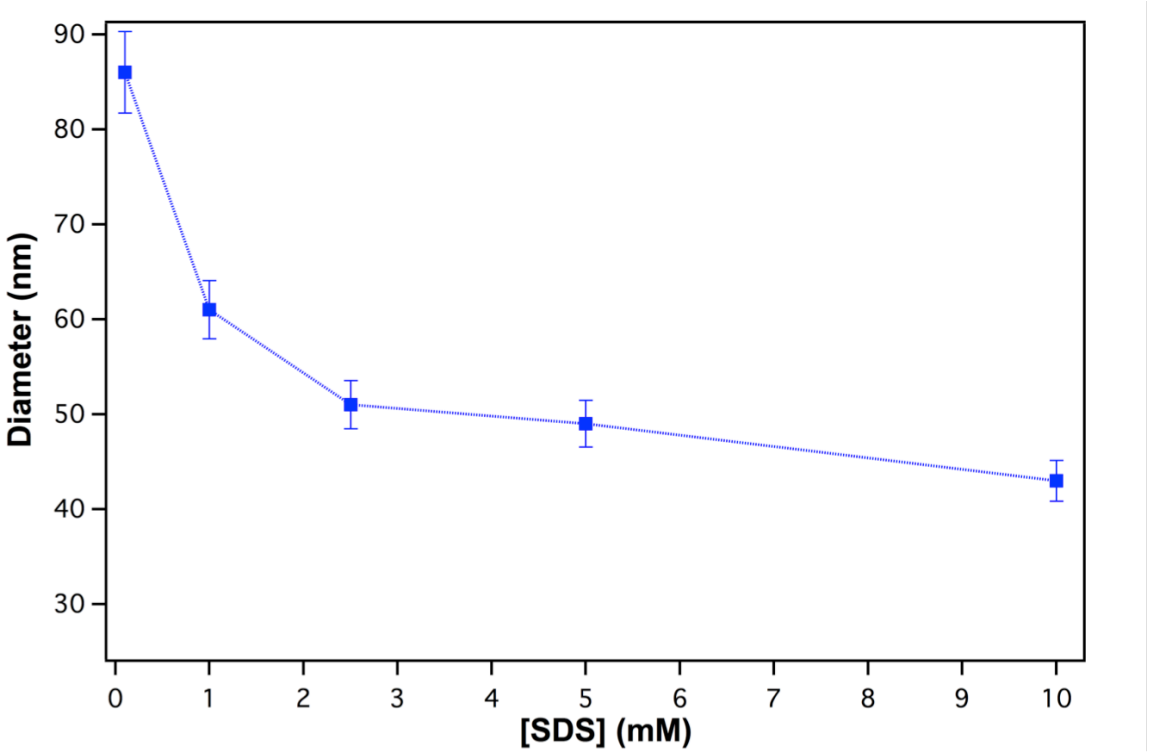

Figure 11: The Effect of Surfactant Concentration on the Mode Nanoparticle Diameter Measured by Nanoparticle Tracking Analysis. P3HT Nanoparticles were Prepared with a Constant P3HT Concentration of 5 mg/mL in Chloroform.

One significant advantage of using the miniemulsion method is the versatility of polymer nanoparticles that can be prepared. As long as the polymer is not soluble in water and is soluble in an immiscible oil phase the method usually can be used. For preparing conjugated polymer nanoparticles this is advantageous because many polymers have been synthesized that are typically soluble in chloroform or chlorobenzene. To demonstrate this versatility, Figure 12 shows nanoparticle solutions that I prepared using the following polymers: poly(styrene) [PS], poly(3-hexylthiophene) [P3HT], poly(benzothiadiazole vinylene) [PBTDV2], poly(cyclopentdithophene benzothiadiazole) [PCPDTBT], poly(benzodithiophene thieno[3,4-b]thiophene] [PTB7]. I was also able to prepare nanoparticles using

commonly used conjugated molecules, e.g., phenyl-C_{61}-butyric acid methyl ester [PCBM] and perylenediimide [PDI].

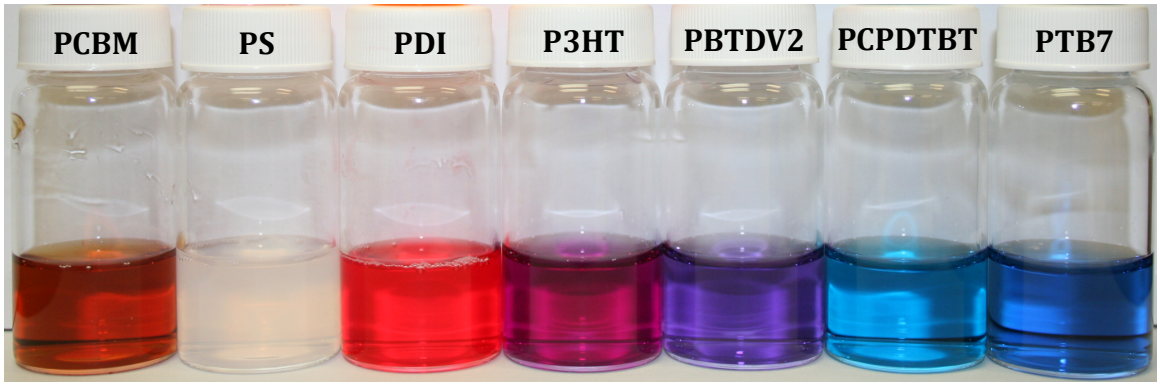

Figure 12: Demonstration of the Versatility of Conjugated Molecules and Polymers that can be Prepared Using the Miniemulsion Method. See the Text for Abbreviations.

To demonstrate further the versatility of this method for preparing organic nanoparticles, I also made P3HT nanoparticles by the standard miniemulsion procedure that I developed, using a variety of commercial products containing surfactants. For these preparations, aqueous SDS solution was substituted by 1:100 volume diluted solutions of Tide laundry detergent, AJAX dish soap, and Suave shampoo & conditioner. Figure 13 shows the nanoparticle solutions prepared with each of these surfactants, and gives the mode nanoparticle size with each surfactant used. It is notable that, despite the fact the commercial products are not pure surfactants – as shown by the fragrance of the samples – still, the characteristic purple dispersion of P3HT nanoparticles was produced, and fairly small nanoparticles were prepared in each case.

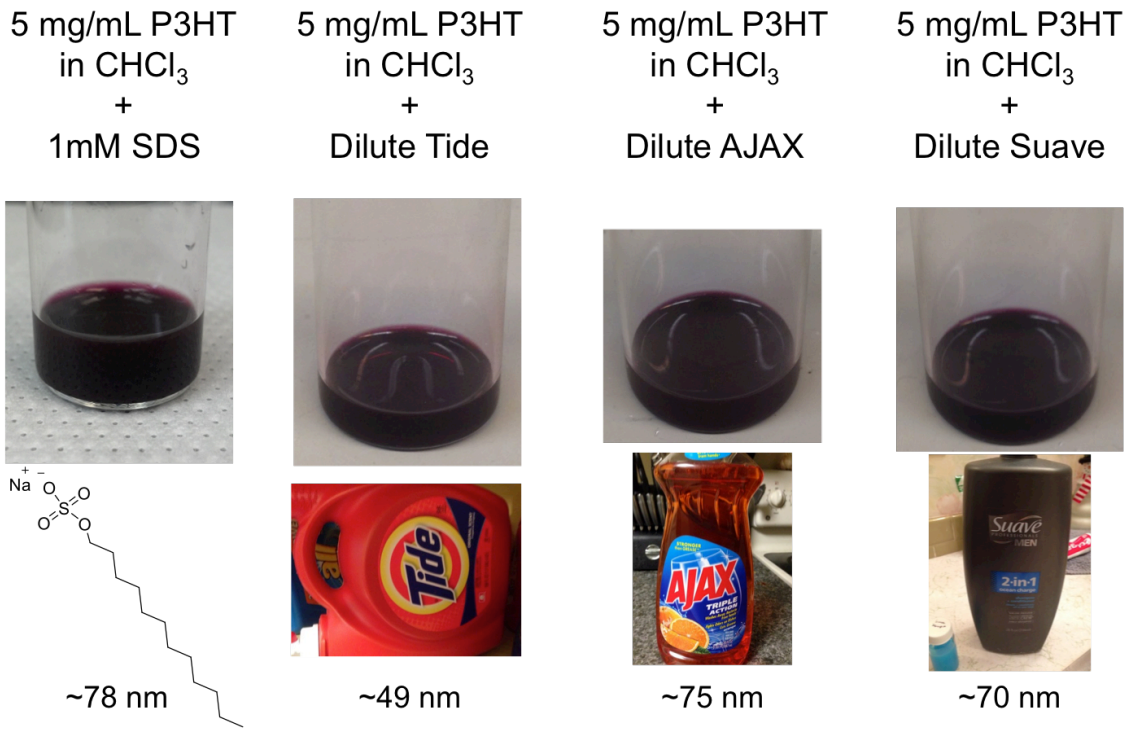

Figure 13: Demonstrating Nanoparticle Miniemulsion Fabrication Products for P3HT, Using Commercial Products Containing Surfactants

Adapted with permissions from Renna, L. A.; Gehan, T. S.; Venkataraman, D. In Optical Properties of Functional Polymers and Nano Engineering Applications; Jain, V., Kokil, A., Eds.; CRC Press: Boca Raton, FL USA, 2014; Vol. 1, pp 227-252.

Members of the DV group have shown that the internal structure of P3HT nanoparticles can be tuned by changing the initial oil phase solvent.[19] Using SDS as the surfactant in water, P3HT nanoparticles were prepared from three solvents: chloroform (good solvent for P3HT), toluene (marginal solvent for P3HT), and a 1:4 volume mixture of toluene to chloroform. The authors used UV-Vis absorption data and single particle photoluminescence decay data to probe the P3HT nanoparticle internal morphology. They concluded that when using chloroform as the solvent, the polymer was conformationally distorted, giving rapid aggregation upon removal of the solvent at 80˚C. Since this temperature is above the boiling point of chloroform,

the polymer cannot be solvent-annealed, which is consistent with the observation of higher dispersity in the aggregate structure within the nanoparticles from chloroform. When toluene is used as the solvent for P3HT, the polymer aggregates before all of the toluene is evaporated, and since the mixture is heated at a temperature below toluene's boiling point, the aggregates have time to solvent-anneal, which could cause tighter packing of the polymer chains as indicated by the fit UV-vis absorption data. When using the mixed system, since it is mostly chloroform it is assumed that the polymers have greater chain mobility, and that toluene evaporation allows aggregates to solvent-anneal slowly, leading to a higher degree of structural order (indicated by the fit UV-vis absorption data) within the particle that from chloroform alone. This work gives an in-depth example of how to tune conjugated nanoparticle morphology during synthesis by the miniemulsion method.

Within this chapter I described how the miniemulsion method was optimized within the DV lab to reproducibly prepare nanoparticles. The miniemulsion method for preparing conjugated polymer/molecule nanoparticles has proven effective to produce nanoparticles with a size range of 30 nm – 180 nm. Previous members within the DV group have shown how the internal structure of the nanoparticles can be tuned by changing the initial oil phase. Controlling the reproducibility of the nanoparticle diameter was a critical factor for my work in this general area. Although typically DLS is used in the literature to determine average nanoparticle diameter, I found that NTA allows for the accurate determination of the mode size diameter and an accurate size distribution, since it is an individual nanoparticle

measurement method. I have shown how the polymer concentration and surfactant concentration can be used to tune the mode nanoparticle diameter. This method is highly versatile for a wide range of conjugated polymers and a wide range of surfactants. Therefore, by the sum of findings of previous group members, combined with my results described in this chapter and in the subsequent chapters, use of the miniemulsion method provides control over the nanoparticle average diameter, polymer choice, and internal packing within each nanoparticle.

CHAPTER 3

UNDERSTANDING CHARGE TRANSPORT THROUGH CONJUGATED POLYMER NANOPARTICLE ASSEMBLIES

3.1 Introduction

We have shown that the organic polymer nanoparticle diameter and internal structure can be successfully tuned. With the long-term goal of preparing organic photovoltaic devices, organic nanoparticle assemblies need to be prepared. This raises many questions and potential obstacles. Most importantly, when these nanoparticles assemble, will the negatively charged and electrically insulating surfactants prevent nanoparticles from coming into contact with each other? If the surfactants repel each other and prevent contact between nanoparticles, charge transport within the nanoparticle assemblies will presumably be prevented. Charge transport through nanoparticle assemblies is essential for efficient photovoltaic response. Therefore, if surfactants prevent inter-nanoparticle contact then effective organic nanoparticle devices could not be prepared. If organic nanoparticles can come in contact with each other, then charge transport should be possible, and using organic nanoparticles could be an effective solution to controlling larger scale morphology in organic photovoltaic and other electronic devices.

To test this, charge transport was measured through assemblies of P3HT nanoparticles as described later in the following section, using the Time-of-flight (TOF) method. TOF is a photo-generated method of measuring charge transport along the same direction that charges are transported in organic photovoltaic

devices, i.e, perpendicular to the surface, and through the thickness of a coated film. Details of TOF methodology are given elsewhere.[48]

3.2 Efficient Charge Transport in Assemblies of Surfactant-Stabilized Semiconducting Nanoparticles

Adapted with permission from Bag, M.; Gehan, T.S.; Algaier, D.D.; Liu, F.; Nagarjuna, G.; Lahti, P.M.; Russell, T.P.; Venkataraman, D. Efficient Charge Transport in Assemblies of Surfactant-Stabilized Semiconducting Nanoparticles *Adv. Mater.* **2013**, 25, 6411-6415. doi: 10.1002/adma.201301302 Copyright (c) 2013 WILEY-VCH Verlag GmbH & Co. KGaA, Weinheim.
http://onlinelibrary.wiley.com/wol1/doi/10.1002/adma.201301302/abstract

In the following section adapted from one of the publications for whose work I was one of the two lead authors, a number of experiments were done by or with assistance from others. I gratefully acknowledge Feng Liu for collecting and analyzing the GIWAXS and GISAXS data, Dr. Monojit Bag for preparing and testing the TOF devices, and Dana D. Algaier for collecting the SEM images for this work.

Semiconducting polymer nanoparticles[26,33,49,50] are a focus of recent research as active materials in sensors,[51-53] optical imaging,[54,55] and optoelectronic devices.[36,56] Recently, there is a growing interest in using conjugated polymer nanoparticles to fabricate the active layer in polymer-based organic photovoltaic (OPV) devices.[24,25,57] One significant advantage in using nanoparticles is that the individual electron-donor and electron-acceptor nanoparticles can be pre-formed with tunable size and internal aggregate structure and then self-assemble into well-defined active layer morphologies for OPV applications.[3,58] Moreover, the active layers can in principle be fabricated over large areas through ink-jet printing or spray-coating of stable nanoparticle dispersions. But, nanoparticle dispersions are

typically stabilized by surfactants to prevent aggregation. Therefore, the general expectation has been that the surfactants might impede charge transport in conjugated polymer nanoparticle (CPN) assemblies, since the surfactants might increase the distance between the particles or create interfacial defects. To realize the full potential of using CPNs to generate active layers for OPV devices, it is imperative to demonstrate that CPN assemblies transport charges efficiently. I and the rest of the coworkers with whom I worked with on this section investigated the impact of surfactants on the charge transport in CPN assemblies, and demonstrated that efficient charge transport can be obtained in surfactant-stabilized semiconducting nanoparticle assemblies.

Poly(3-hexylthiophene) was chosen as the conjugated polymer for our studies because it is well-studied in terms of charge mobility[59-61] and molecular packing,[62-64] allowing direct comparison of our measurements with the literature to understand better the impact of surfactants on charge transport. Polymer nanoparticles were synthesized by miniemulsion with different concentrations of sodium dodecyl sulfate (SDS).[65] Two commercially available P3HT samples were used: 93% regioregular P1 with molecular weight 72 kDa and dispersity Đ=2.5; and 97% regioregular P2 with molecular weight 30 kDa and Đ=1.8. Charge carrier mobilities of spray-coated nanoparticle assemblies and drop-cast thin films on the indium tin oxide (ITO) substrates were determined using the time of flight (TOF) method. The thicknesses of the films were measured by profilometry. Further details are provided in the experimental section of this dissertation.

Figure 14a shows the transient photocurrent, [$I_{ph}(t)$], in traces at different applied fields for spray-coated nanoparticle assemblies obtained from a non-centrifuged P1 nanoparticle dispersions containing 1 mM SDS. The average size of these nanoparticles estimated from dynamic light scattering was 145 nm. The film thickness, as measured by profilometer was 0.5±0.05 μm. From this thickness of the sample (d), the transit time (τ_{tr}) and the applied bias voltage (V), the charge carrier mobility (μ) can be calculated using Equation 1.

$$\mu = d^2/V\,\tau_{tr} \qquad (1)$$

Within the photocurrent transient trace in Figure 14a there are two distinct linear regions. The transit time was taken as the tangential intersection of these linear regions. For efficient charge transport through polymer thin films, the slope of the first linear region (S1), at $t<<\tau_{tr}$, should be close to zero and the slope of the second linear region (S2), at $t>>\tau_{tr}$, should be a large negative number. This is typically observed for trap-free charge transport[66] and has been interpreted as being related to "charge carrier hopping within a Gaussian density of states under moderate energetic disorder".[67] A totally dispersive transport — i.e., trap-state limited — will yield S1 = S2 = –1. The hole transport through the P1 nanoparticle film shows a weak dependence on the applied field. The hole mobility was $\sim 10^{-4}$ $cm^2V^{-1}s^{-1}$, comparable to pristine P3HT thin film hole mobility reported in the literature.[61,68,69] The nanoparticle TOF transients show more dispersive transport (S1 = –0.7, S2 = –1.4) than seen in typical P3HT thin film devices. We therefore concluded that the charge transport through these polymer nanoparticle films is trap-state limited.

The scanning electron microscopy images of films spray-coated from the nanoparticle dispersions with excess surfactants (Figure 14b), show a low packing fraction and poor structural order. The images also show the presence of excess surfactants at the air interface. Based on these results, we concluded that the trap-states arise from the excess surfactant and structural disorder in the nanoparticle assemblies. In films spray-coated from a dispersion of P1 nanoparticles with 16 mM SDS, the TOF hole mobility was $\sim 10^{-5}$ $cm^2V^{-1}s^{-1}$. These results indicate that the hole mobility decreases with increasing surfactant concentration. However, the surfactants do *not* prohibit the transport of charges.

The excess SDS was removed by multiple centrifugal filtrations as described in the experimental section. The centrifugation cycles were continued until no precipitation was observed in the filtrate when it was treated with $BaCl_2$(aq). The zeta potential of the nanoparticles remained at –60 mV after each cycle, indicating that the centrifugation process only removes excess surfactant and not the surfactant layers coating the nanoparticles.

Figure 14c shows the photocurrent transient in a spray-coated thin film prepared from the centrifuged P1 nanoparticle dispersion. From TOF, a hole mobility of $\sim 10^{-4}$ $cm^2V^{-1}s^{-1}$ was calculated; it had a weak bias dependence. From the slopes of the two linear regions in the photocurrent transient, we found that S1 = –0.23 and S2 = –1.9 respectively. Although the hole mobility is on the same order of magnitude as that for the non-centrifuged nanoparticle film, the change in S1 and S2 slopes indicates a less dispersive transport through the nanoparticle film from which the excess surfactant was removed.

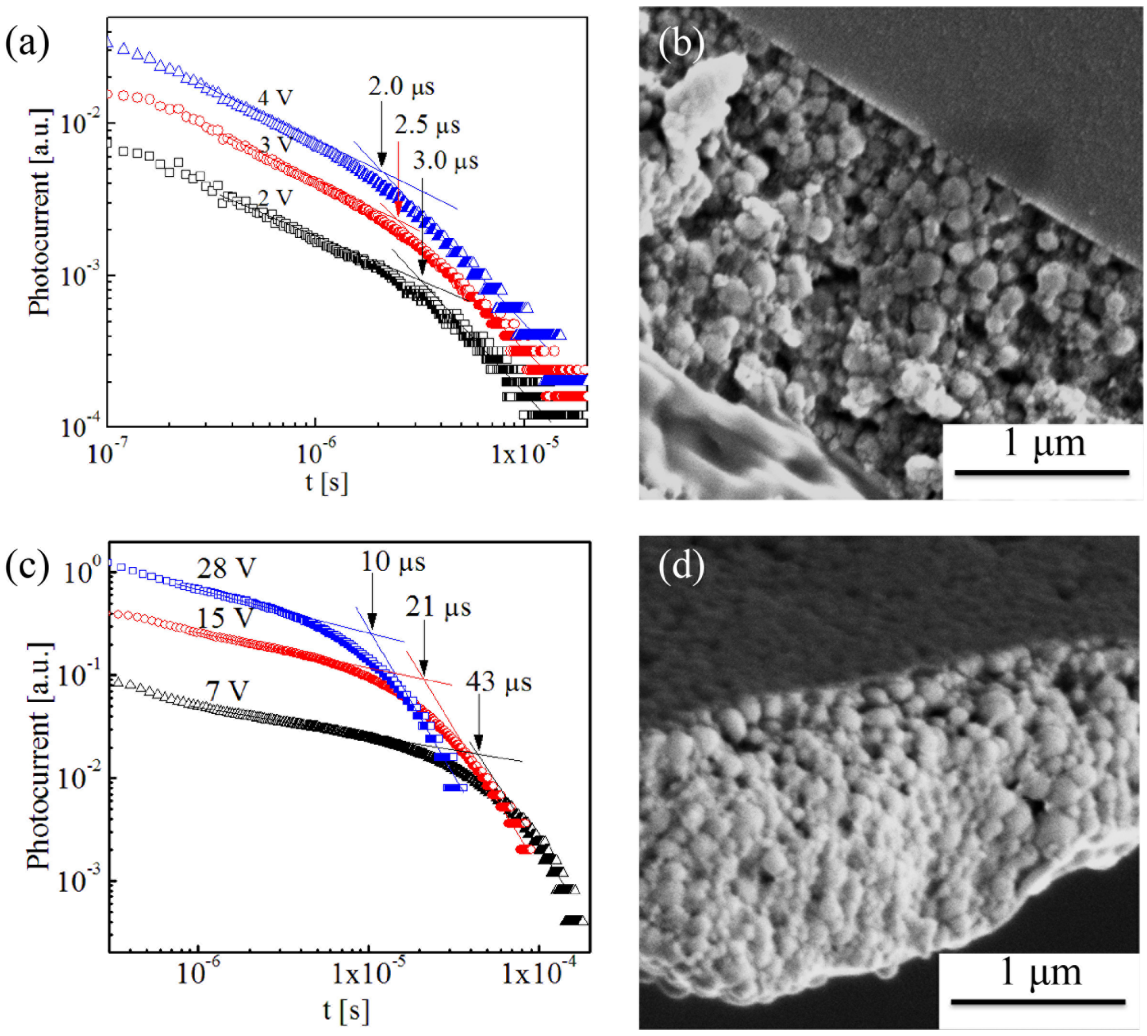

Figure 14: (a) Transient Photocurrent from a Non-Centrifuged P3HT (P1) Nanoparticle Film Synthesized from 1mM SDS Surfactant. Nanoparticles Were Spray-cast on a ITO Coated Glass Substrate, Giving a Film Thickness of ~0.5 µm by Profilometry. (b) Cross-sectional SEM Image of a Film Made as for Chart (a), but Coated on a Si substrate. (c) Electric Field Dependent Transient Photocurrent at 30°C from a Spraycaste Nanoparticle Film After Centrifugation of Polymer P1. Film Thickness was 2.5 µm. (d) Cross-sectional SEM Image of a Centrifuged Sample of P1 Nanoparticles Spray-cast on a Si Substrate

To compare with thin films, a centrifuged P1 sample was drop cast from hot chlorobenzene and annealed at 150˚C for five minutes. A comparison of normalized photocurrent transients is shown in Figure 15a for the spray-coated non-centrifuged nanoparticle film, the spray-coated centrifuged nanoparticle film, and

the drop-cast thin film of P1. The thin film photocurrent transient is very similar to that of P3HT TOF transients reported in literature, with S1 = –0.07 and S2 = –2.0. Figure 15a clearly shows that removing the excess surfactant from the nanoparticle dispersion gives a spray-coated nanoparticle film with hole transport that becomes less dispersive and comparable to that of a P1 pristine thin film. Notably, the hole mobilities of the nanoparticle spray-coated films of polymer P1 and P2 are comparable to that of a pristine polymer thin film [Figure 15b].

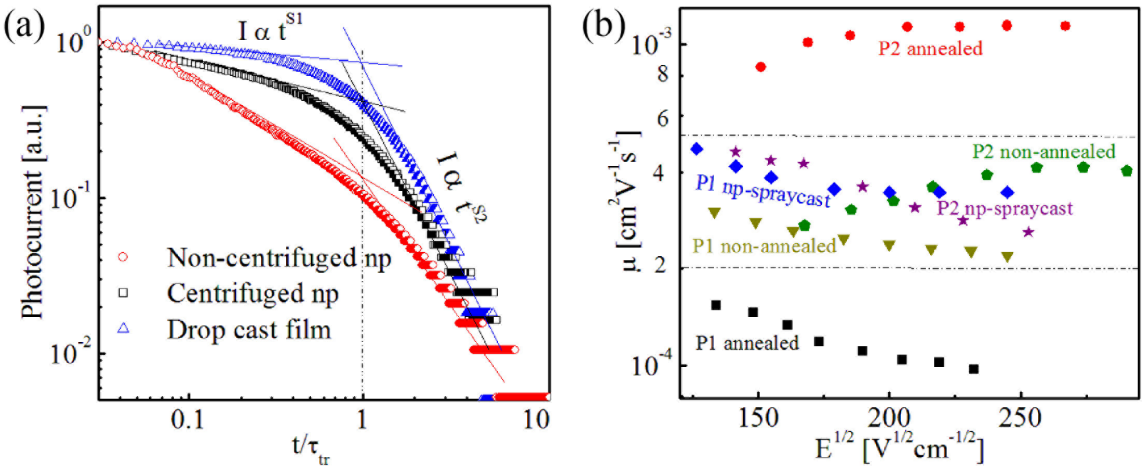

Figure 15: (a) Transient Photocurrent Response from Three Test Devices Made with the P1 Sample of P3HT: (Δ) Drop-cast, (□) Centrifuged Sample Spray-cast, and (¢) Non-centrifuged Sample Spray-cast. Time Scales are Normalized with Respect to Transit Time τ_{tr}. (b) Electric Field Dependent Mobilities Estimated from Different P3HT Materials. P1 (***M*** $_w$ **= 72 kD, rr = 92%, Đ = 2.5) and P2 (***M*** $_w$ **= 30 kDa, rr = 97%, Đ = 1.8). Results Listed as "Annealed" Were Drop-cast Films from Chlorobenzene Annealed at 150°C for 5 min Under Nitrogen. Nanoparticles Were Spray-cast at 80°C After Centrifugation.**

The origin of efficient charge transport in a spray-coated film from centrifuged nanoparticle dispersion was also investigated structurally. Strong (100) and (020) diffraction rings, seen in the in-plane as well and out-of-plane grazing incidence wide angle x-ray scattering (GIWAXS) [Figure 16a & Figure 16b], are

characteristic of the inter-chain packing of the P3HT chain and the π- π stacking of the thiophene ring within the nanoparticles. These rings are quite uniformly distributed in all azimuthal angles, indicating no crystal orientation preference. This observation is quite different from common spin-coated P3HT thin film sample, which predominately takes an edge-on orientation relative to the substrate. A rapid decrease in the intensity of the GISAXS [Figure 16c] indicates that the nanoparticle spray-coated films are structurally similar to a drop-cast P3HT thin film, while the SEM image in Figure 15d clearly shows close-packed nanoparticles. An average particle-particle distance of ~220 nm for a non-centrifuged sample and ~130 nm for a centrifuged sample, were determined from a Fourier Transform of the SEM images [Figure 16d-f]. Based on these data, we conclude that nanoparticles pack much more closely in a spray-coated film from a centrifuged dispersion than from a film spray-coated from a non-centrifuged dispersion. Consequently we can attribute the improved charge transport in nanoparticles assemblies without excess surfactants to a closer packing of the nanoparticles.

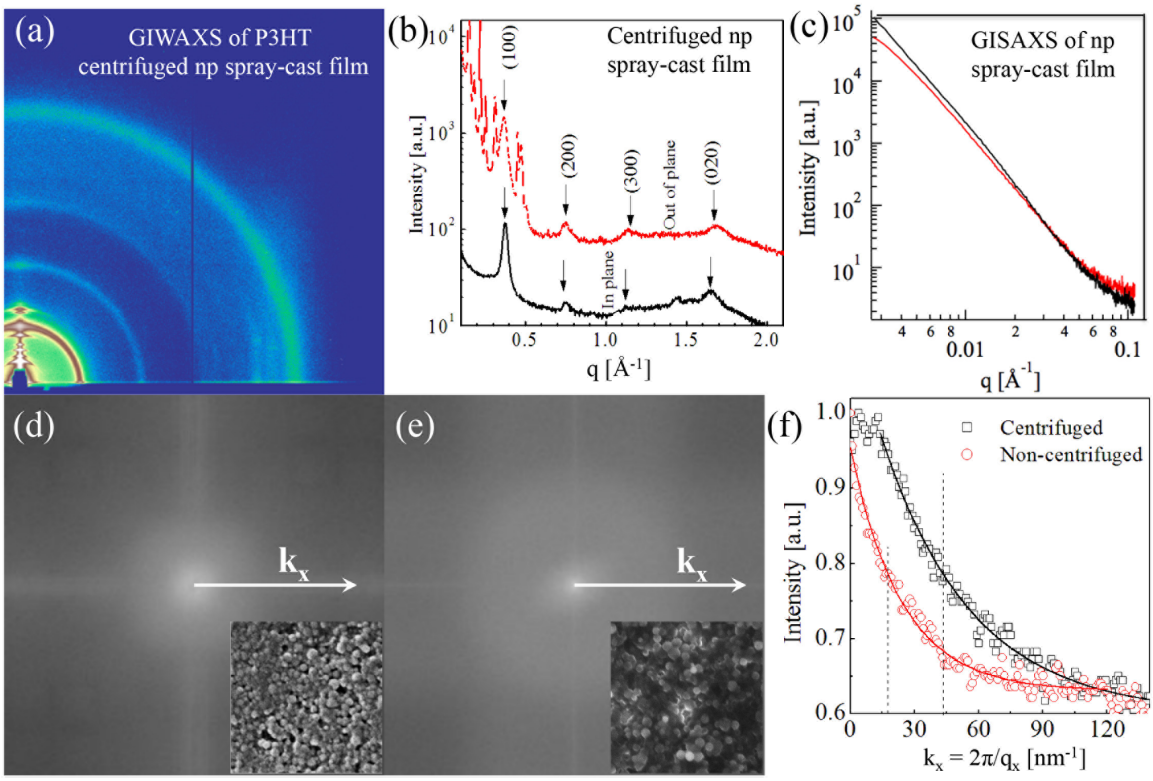

Figure 16: (a) GIWAXS Diffractogram of a Centrifuged Spray-cast Film (b) Intensity Profile of GIWAXS Reflection Image Showing Various Crystal Planes; (c) GISAXS of Centrifuged and Non-centrifuged Nanoparticle Spray-cast Samples; (d & e) Fourier Transform of SEM Images of Centrifuged and Non-centrifuged Nanoparticle Samples (f) Intensity Profiles Along the Direction k_x.

The hole transport in P3HT thin films is also affected by the molecular weight and regioregularity of the polymer. To probe these effects in the nanoparticle assemblies centrifuged nanoparticle dispersions of P1 and P2 sample were spray-coated onto an ITO substrate and the TOF hole mobility was measured. As shown in Figure 15b, non-annealed drop-cast thin films of P1 and P2 both have hole mobilities of ~3×10^{-4} $cm^2V^{-1}s^{-1}$. Upon annealing films of P1 — the high molecular weight and less regioregular P3HT — the hole mobility drops to ~1×10^{-4} $cm^2V^{-1}s^{-1}$. For P2 — the low molecular weight and highly regioregular P3HT — the hole mobility increases to ~1×10^{-3} $cm^2V^{-1}s^{-1}$. The two distinct behaviors found upon

annealing the drop-cast films of P1 and P2 can arise from different orientations of π–π stacking onto the substrates. Similar molecular weight dependent structure-related properties have also been observed in FET measurements of P3HT.[70] The nanoparticle spray-coated films of P1 and P2 have a hole mobility of $\sim 4\times10^{-4}$ $cm^2V^{-1}s^{-1}$ indicating more isotropic crystal orientation in the spray-coated film.

Surfactant-stabilized P3HT nanoparticle dispersions were synthesized by the miniemulsion technique and their spray-coated films were characterized by TOF mobility measurements. Although the hole mobilities of the spray-coated films from non-centrifuged P3HT nanoparticle dispersions are comparable to a drop-cast thin films of pristine P3HT, the hole transport through the nanoparticle films is highly dispersive. Upon removal of the excess surfactant by a centrifugal filtration, the nanoparticles yield films in which hole transport becomes less trap-state limited, less dispersive, in comparison to the non-centrifuged nanoparticle film, and is comparable to behavior seen in pristine P3HT films. This improved hole transport is attributed to a higher packing density in the centrifuged nanoparticle spray-coated films due to removal of the excess surfactant. Although P1 and P2 have different molecular weights and regioregularities, they show similar hole transport behavior in spray-coated nanoparticle films. With this demonstration of effective charge transport within nanoparticle films, the nanoparticle assembly approach shows much promise for fabricating organic electronic devices with high reproducibility from a wide variety of polymeric materials without major modification of processing parameters.

CHAPTER 4

ORGANIC NANOPARTICLE PHOTOVOLTAICS

4.1 Introduction

Keeping the long-term goal in mind of using organic nanoparticles to control the morphology in organic photovoltaic devices, assemblies of two types of nanoparticles have to be prepared. It was shown in section 3.2 that charges can be efficiently transported through assemblies of P3HT nanoparticles alone. This is a significant step because we have shown that an insulating surfactant surrounding nanoparticles does not prevent charge transport through assemblies of P3HT nanoparticles. But, for an effective photovoltaic response active layer, we would need two types of nanoparticles, comprising an electron donating material and an electron accepting material. Also, the active layer in efficient organic photovoltaic devices are typically around 150 nm – 250 nm thick uniform films on top of a PEDOT:PSS coated ITO substrate. So our goal was to develop a method to prepare uniform films of a binary assembly of semiconducting nanoparticles in an aqueous solution. The progress that I made toward this goal is described below.

4.2 Switching from Spray-coating to Spin-coating to Prepare Uniform Binary Nanoparticle Films from Aqueous Solutions.

Bag, M.; Gehan, T.S.; Renna, L.A.; Algaier, D.D.; Lahti, P.M.; Venkataraman, D. Fabrication Conditions for Efficient Organic Photovoltaic Cells from Aqueous Dispersions of Nanoparticles. *RSC Adv.* **2014**, 4, 45325-45331 - Adapted with permission of The Royal Society of Chemistry

In the following section adapted from one of the publications for whose work I was one of the two lead authors, a number of experiments were done by or with

assistance from others. I gratefully acknowledge Dr. Monojit Bag for preparing / testing the TOF devices and preparing / testing the photovoltaic devices, Dana D. Algaier for collecting the SEM images for this work, and Lawrence A. Renna for collecting the AFM data.

In the previous section spray-coating was used to prepare films for TOF measurements. These nanoparticle films were prepared using a commercial Omni 5000 airbrush, and the nanoparticle solution was sprayed onto ITO coated glass substrates set on a hot plate at ~80 – 85 °C. Enough nanoparticle solution was sprayed until a thickness of at least 1 μm. This is described in further detail in Chapter 6.3.1. Spray coating prepared nanoparticle films with a film roughness that was acceptable for TOF measurements, but it was quickly determined that spray-coating gave films that were too rough when coated on top of the PEDOT:PSS film. Therefore, we switched to spin-coating because it is commonly used to prepare uniform polymer films consistently with sub-micron thickness. More details of the spin-coating process are described in Chapter 6.2.

Spin-coating polymer films waste a lot of polymer in solution because much of the solution is spun off the coated substrate. Therefore, high concentrations of active layer materials typically need to be used. Therefore, concentrated polymer nanoparticle solutions were prepared following the procedure described in section 6.1, mixing 0.5 mL of 30 mg/mL of polymer solution with 3.0 mL of 10 mM aqueous SDS solution. Two of these nanoparticle dispersions were prepared and added to a centrifugal filtration tube with a 5kDa molecular weight cutoff (MWCO), although it was later determined that a 10kDa MWCO also works to remove surfactant with

faster centrifugation. To remove the excess surfactant in solution, the nanoparticle dispersion underwent two centrifugation cycles and was re-suspended in water with dilution to 0.5 mL. A film of P3HT nanoparticles only can be made by initially adding two P3HT nanoparticle solutions to a centrifugal filtration tube. If a binary nanoparticle film is desired, then one P3HT nanoparticle solution and one PCBM nanoparticle solution can be centrifuged, or a desired volume ratio of P3HT and PCBM nanoparticles combined for centrifugation. Also two solutions of "blend" nanoparticles can be used, where both P3HT and PCBM are blended in each nanoparticle. Blend nanoparticles were used initially as the concentrated nanoparticle / polymer solution for preparing nanoparticle films by spin-coating.

The concentrated nanoparticle solution of semiconducting polymer or polymer/PCBM mixture was initially spin-coated at a wide range of spinning speeds onto a PEDOT:PSS coated ITO substrate in attempt to prepare a uniform nanoparticle film. Spin-coating these concentrated nanoparticle solutions typically formed large aggregates, as shown in the optical image in Figure 17a. It was observed that the aqueous nanoparticle solution did not wet the PEDOT:PSS surface very well, with an estimated advancing angle $\theta_A \approx 15°$ and a receding angle $\theta_R \approx 8°$. This was initially confusing, since PEDOT:PSS is hydrophilic and spin-cast from an aqueous solution itself. Multiple concentrations of polymer solution and multiple spinning speeds all typically led the same result: "patchy", rough films with large aggregates of nanoparticle. A uniform film is required for an efficient photovoltaic response.

Serendipitously, a set of PEDOT:PSS coated ITO substrates were left exposed to atmospheric conditions at room temperature all weekend. It was observed that the concentrated nanoparticle solution wet this PEDOT:PSS surface and spread easily across the substrate surface. After much deliberation of what could have happened to change the substrates surface properties, we hypothesized that the polymer surface could have oxidized over the weekend, making it more hydrophilic. To test this hypothesis we intentionally oxidized the surface by preparing PEDOT:PSS coated ITO substrates and immediately treating them with UV-O_3, which should oxidize some of the double bonds of the polymer on the surface and make it more hydrophilic. The concentrated nanoparticle solution wet the UV-O_3 treated substrates much better, with an advancing angle $\theta_A < 2°$. Upon spin-coating these substrates, the nanoparticle films visually were much more uniform, as shown by the optical microscopy image in Figure 17b. Before UV-O_3 treatment, the film's root mean squared (rms) roughness was ~ 70 nm (from the AFM image in Figure 18a) which is close to the average diameter of the nanoparticles used (~80 nm). After UV-O_3 treatment, the film's rms roughness drops to ~14 nm (from the AFM image in Figure 18c).

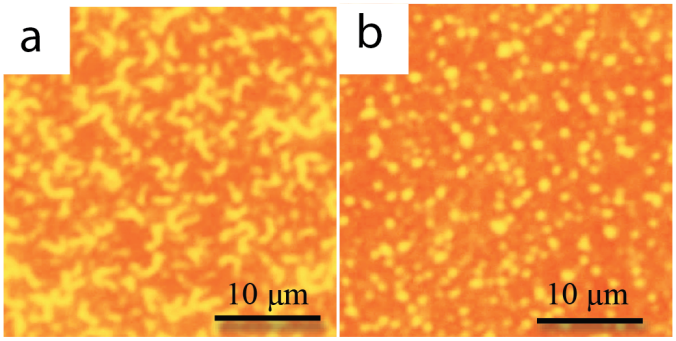

Figure 17: Transmission Mode Optical Microscopic Image of P3HT:PCBM Blend-Nanoparticle Sample Spin Coated on (a) As-Prepared PEDOT:PSS Coated ITO Substrate; (b) UV-O_3 Treated PEDOT:PSS Coated ITO Substrate.

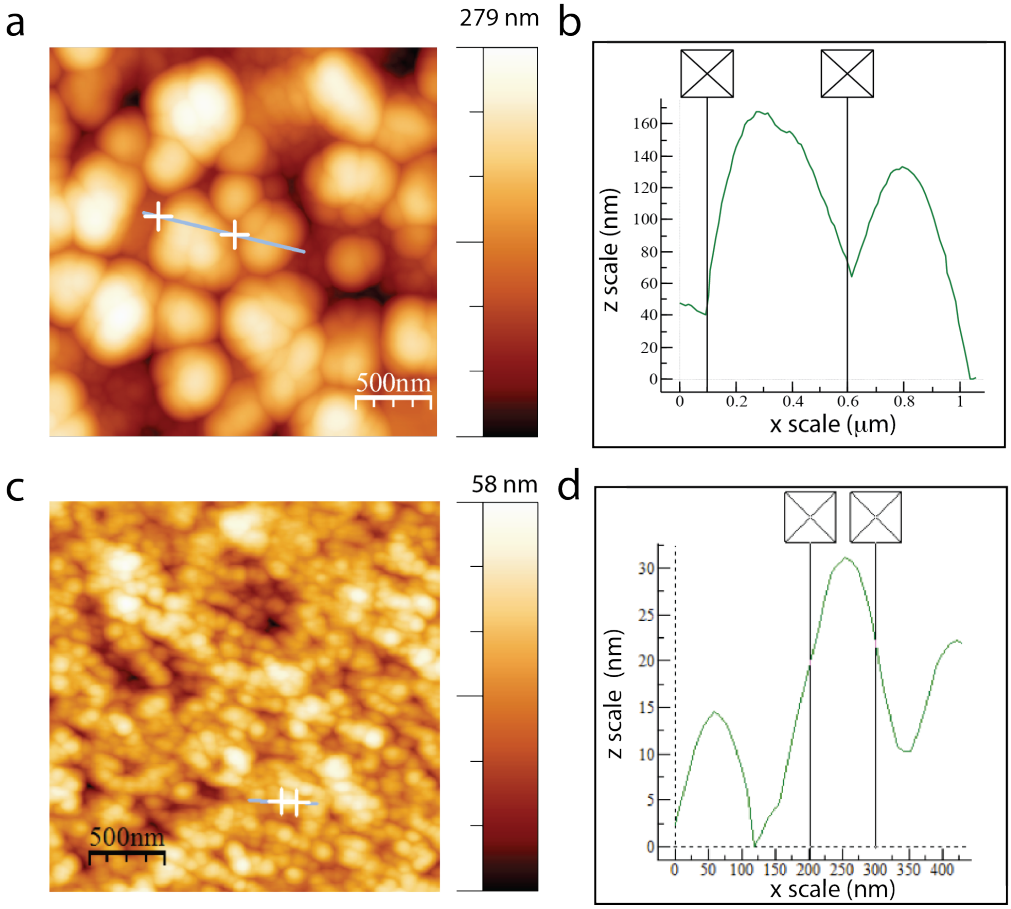

Figure 18: (a) AFM Image of P3HT:PCBM Blend-Nanoparticle Film, Spin-Coated on As-Prepared PEDOT:PSS Coated ITO Substrate. Average rms Roughness is ~70 nm. (b) Line Profile of the AFM Image Showing Sub-micrometer to Micrometer Range of Particle Aggregates. (c) AFM Image of P3HT:PCBM Blend-Nanoparticles Film Spin Coated on UV-O3 Treated PEDOT:PSS Coated ITO Substrate. Average rms Roughness is ~14 nm. (d) Line Profile of the AFM Image in (c) Showing Nanoparticle Diameters of the Order of 100 nm. The Crosses in the Line Profile Correlate to the Crosses in AFM Image in (c).

4.2 Preparing Efficient Nanoparticle Organic Photovoltaic Devices

Adapted and Reprinted with permission from Gehan, T.S.; Bag, M.; Renna, L.A.; Shen, X.; Algaier. D.D.; Lahti, P.M.; Russell, T.P.; Venkataraman, D. *Nano Letters* **2014** 14 (9), 5238-5243. Copyright 2014 American Chemical Society.

In the following section adapted from one of the publications for whose work I was one of the two lead authors, a number of experiments were done by or with assistance from others. I gratefully acknowledge Dr. Monojit Bag for preparing / testing the TOF devices and preparing / testing the photovoltaic devices, Dana D. Algaier and Xiaobo Shen for collecting the SEM images for this work, and Lawrence A. Renna for collecting the AFM data and performing the computed random assembly of spheres simulations.

Conjugated polymer NPs have been investigated as active layer materials in organic photovoltaics (OPVs), albeit with limited success.[24,28,57,71] This work shows that efficient OPVs can be fabricated with blend NPs *and* with separate component NPs using P3HT and PCBM, the archetypical active layer materials in OPVs,[4] by combining the principles of sphere packing with improved fabrication methods. Blend NPs have electron- and hole transporters in the same NP, offering a unique pathway to create bulk heterojunction (BHJ) structures within a single NP,[71-73] and to propagate this structure to the mesoscale through self-assembly. On the other hand, formulating active layer materials into separate NPs prior to their co-assembly allows the control of their size, their internal structure and ordering, and their surface properties. These attributes enable the formation of domains having pre-defined sizes, independently tailored ordering, and well-defined contacts (interfaces) between the electron and hole transporting domains. Therefore this

method offers control over polymer and molecule packing all the way from the molecular scale through the nanoscale, and including the mesoscale packing of a blend of these active layer materials, as described in Figure 19.

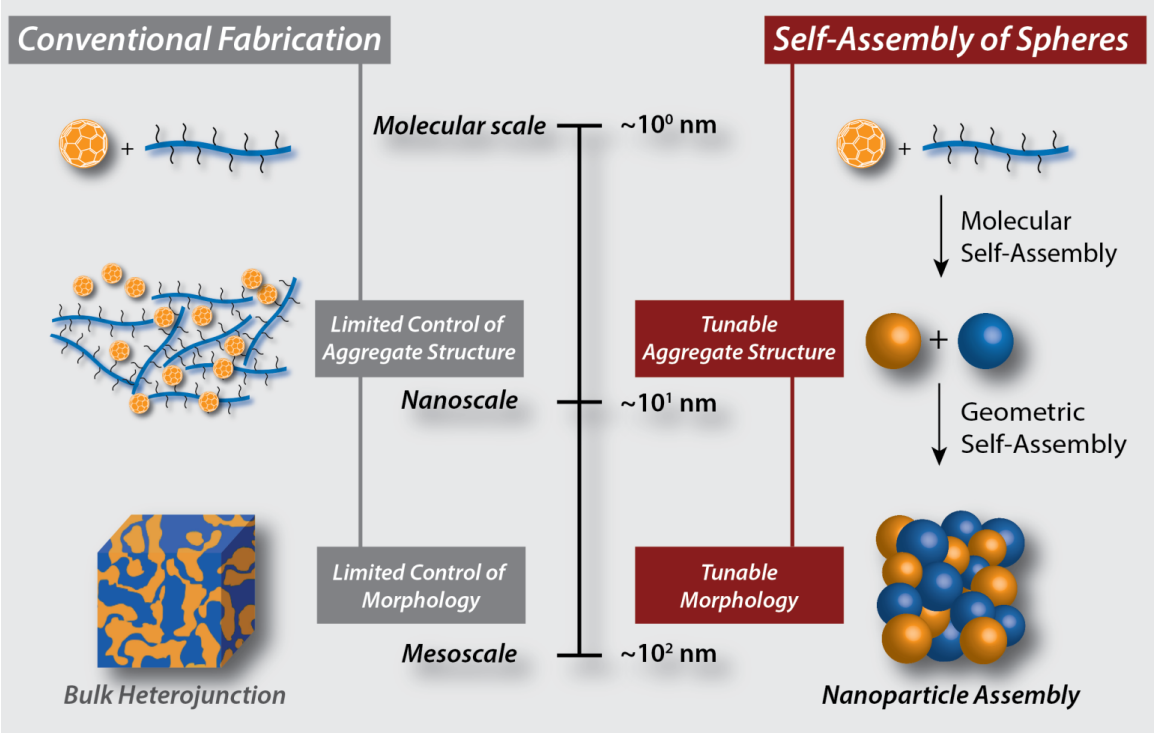

Figure 19: Schematic comparison of morphology control with the conventional method and the NP assembly method for the fabrication of organic photovoltaic active layers.

4.2.1 Nanoparticle Synthesis and Characterization in Solution and as Assemblies

The blend NPs and separate NPs were fabricated using a modified mini-emulsion method.[19,38] The diameter of the blend NPs was determined to be 80±9 nm using nanoparticle-tracking analysis (NTA). The diameter of P3HT NPs was 79±20 nm and PCBM NPs was 71±24 nm. The diameter from a 1:1 number ratio mixture of separate component P3HT and PCBM NPs was 74±11 nm indicating that there was

no aggregation of the NPs in the dispersion. The molecular packing of P3HT in aqueous NP suspensions was probed using electronic spectroscopy. The UV-vis spectrum of P3HT can be deconvoluted into absorption arising from aggregate P3HT and from amorphous P3HT.[19] Deconvolution details are given in the literature.[19] Using this method, we estimated that in P3HT:PCBM blends *and* in separate P3HT NPs, the ratio of aggregate to amorphous P3HT was 70:30, Figure 20. We attribute the amorphous component to P3HT within the NP and not to free P3HT, because P3HT is insoluble in water. Since blend and separate NPs show similar ratios of aggregate to amorphous P3HT, we conclude that adding PCBM does not significantly affect P3HT aggregation in the blend NPs. In a bulk heterojunction (BHJ), the PCBM is expected to concentrate in the amorphous or non-aggregated domains of P3HT or to phase separate from P3HT.[7,8] The UV-vis spectra of both blend NP and separate NP dispersions having similar particle sizes and concentrations show features similar to those of annealed thin films of admixed blend P3HT and PCBM cast from chlorobenzene. The P3HT aggregate in P3HT-only nanoparticles is estimated to be 71%. When the PCBM nanoparticle absorption was subtracted from the blend absorption spectrum to estimate P3HT amorphous and aggregate absorption, the P3HT aggregate in the blend nanoparticles is 70%. These results indicate that the same aggregation features formed in thin films can be captured in the nanoparticles. X-ray diffraction (XRD) of blend and separate nanoparticle assemblies show similar results indicating crystalline P3HT formation within the nanoparticles (Figure 21), based on the observed, relatively sharp and strong diffraction peaks.

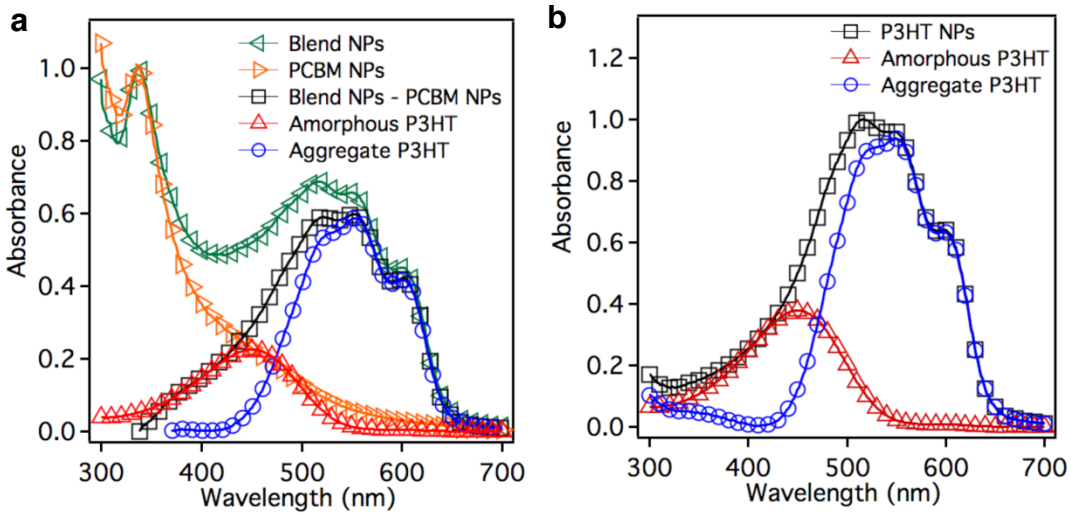

Figure 20: (a) P3HT:PCBM Blend Nanoparticle Absorption Spectra. PCBM NPs Absorption was Subtracted from the Blend Absorption Spectrum to Estimate P3HT (Amorphous and Aggregate) Absorption. P3HT Aggregate in the Blend NPs is 70.22%. (b) P3HT Nanoparticle Absorption Spectra. P3HT Aggregate in the NPs is Estimated to be 71.25%.

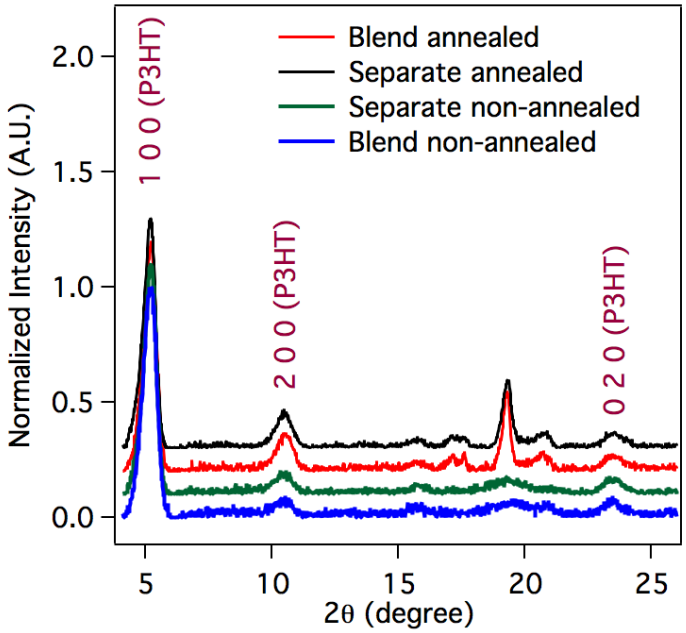

Figure 21: X-ray Diffraction Data for P3HT and PCBM Blend and Separate Nanoparticle Films Drop-Cast Under Infrared Lamp. Enhanced PCBM Peak is Observed After Ramp Heating (Annealing) from 30°C to 150°C Temperature Under Nitrogen Atmosphere. A Strong 100 P3HT Peak is Observed in All Samples.

Scanning electron microscopy (SEM) images of spin-coated assemblies of blend nanoparticles (NPs) and co-assemblies of separate P3HT and PCBM NPs (1:1 number ratio) on silicon substrates show that the NPs form jammed assemblies with close particle-particle contacts (Figure 22c). A simulation[74] of a random close packed co-assembly of two types of hard spheres (Figure 22a) having the same radii in a 1:1 number ratio shows interconnected pathways for both types of particles. These interconnected pathways are clearly seen in Figure 22b where all the spheres of one type from Figure 22a are omitted. To differentiate experimentally between P3HT and PCBM NPs, the same film from Figure 22c was dipped into dichloromethane for 15 min to remove the PCBM selectively. A SEM image of the resultant film is shown in Figure 22d. The binary images in Figure 22e and Figure 22f of Figure 22c and Figure 22d, respectively, show removal of approximately half of the NPs. After this removal of PCBM NPs, the void spaces in the film are visible, demonstrating that the films are a jammed co-assembly of P3HT and PCBM NPs. Cross sectional SEM of a thin film of P3HT:PCBM blend NPs confirms that the NPs are closely packed throughout the film. Similar results were also observed for separate NP co-assembled active layers.

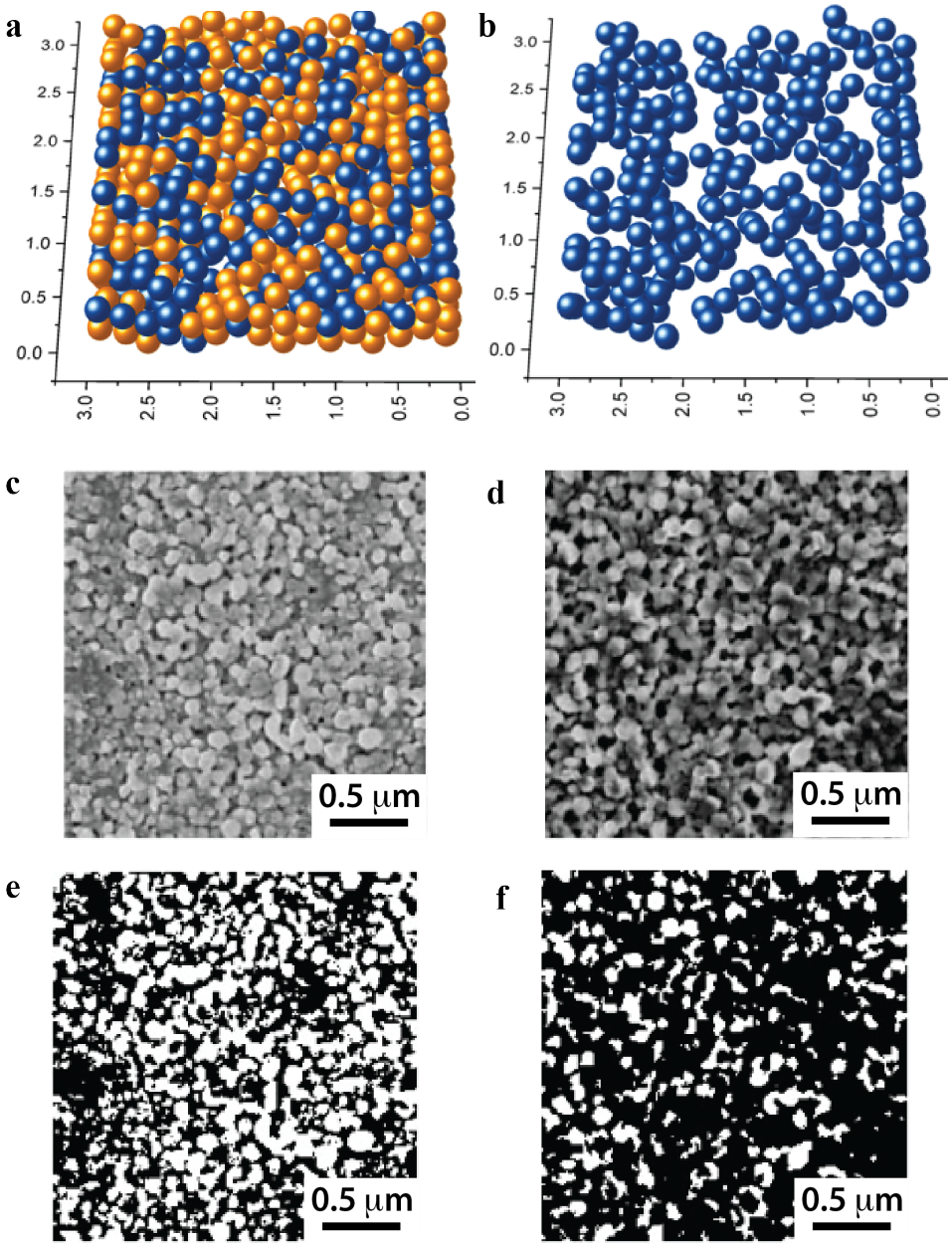

Figure 22: (a) Simulated Packing of a 1:1 Number Ratio of Two Types of Particles Showing Random, Jammed Assembly. (b) Simulated Packing of a 1:1 Number Ratio of Two Types of Particles Showing Conducting Pathways for One Set of Particles (Other Type is Omitted). (c) Top View SEM of P3HT and PCBM Separate NPs. (d) Top View SEM of P3HT and PCBM Separate NPs Washing with DCM for 15 min. (e) A Binary Scale Image of the SEM image in c. (f) A Binary Scale Image of the SEM Image in d.

4.2.2 Electronic Characterization of Nanoparticle Assemblies using Conducting Atomic Force Microscopy and Time-of-Flight

Conducting AFM (cAFM) was used to probe the conducting pathways in the active layer of the NP films made in these studies. cAFM images of assemblies of blend NPs and co-assemblies of separate NPs (~240 nm thick films) on ITO/PEDOT:PSS are shown in Figure 23. Based on the applied bias conditions, the measured current is a result of the movement of holes to the platinum probe. The dark red regions in the images are areas of high hole conductivity and the blue regions are areas of low hole conductivity. Both Figure 23a (blend NPs) and Figure 23b (separate NPs) show the presence of conductive pathways for hole transport through the NP films to the platinum probe. In control testing, cAFM of films composed only of P3HT NPs or PCBM NPs show uniformly high conductivity throughout the film for the former, and uniformly low conductivity for the latter; this corresponds to high and low hole transport in the respective films (Figure 24). Therefore, we conclude that the areas of low current are regions with either a high concentration of PCBM or regions surrounded by PCBM. All of these results show that there are continuous pathways for hole transport in random assemblies of both blend and separate NPs.

Histograms of the current mapping provide clues to the underlying device morphology; the number of counts is directly proportional to the number of available paths in the film for hole conduction, and the current is related to path length from a given particle to the ground electrode. The histogram analysis (Figure 23c) of Figure 23a and Figure 23b show the morphological difference between the blend and separate NP films. They also show that the separate NP film has a slightly

larger average normalized current than the blend NP film. The current distribution peak width is larger for separate NPs than it is for blend NPs, indicating a wider distribution of pathways including more short pathways having low resistance. The cAFM results show that (a) there are conductive pathways for holes through the bulk of both blend and separate NP films, and (b) there are morphological differences between active layers derived from blend versus from separate NPs.

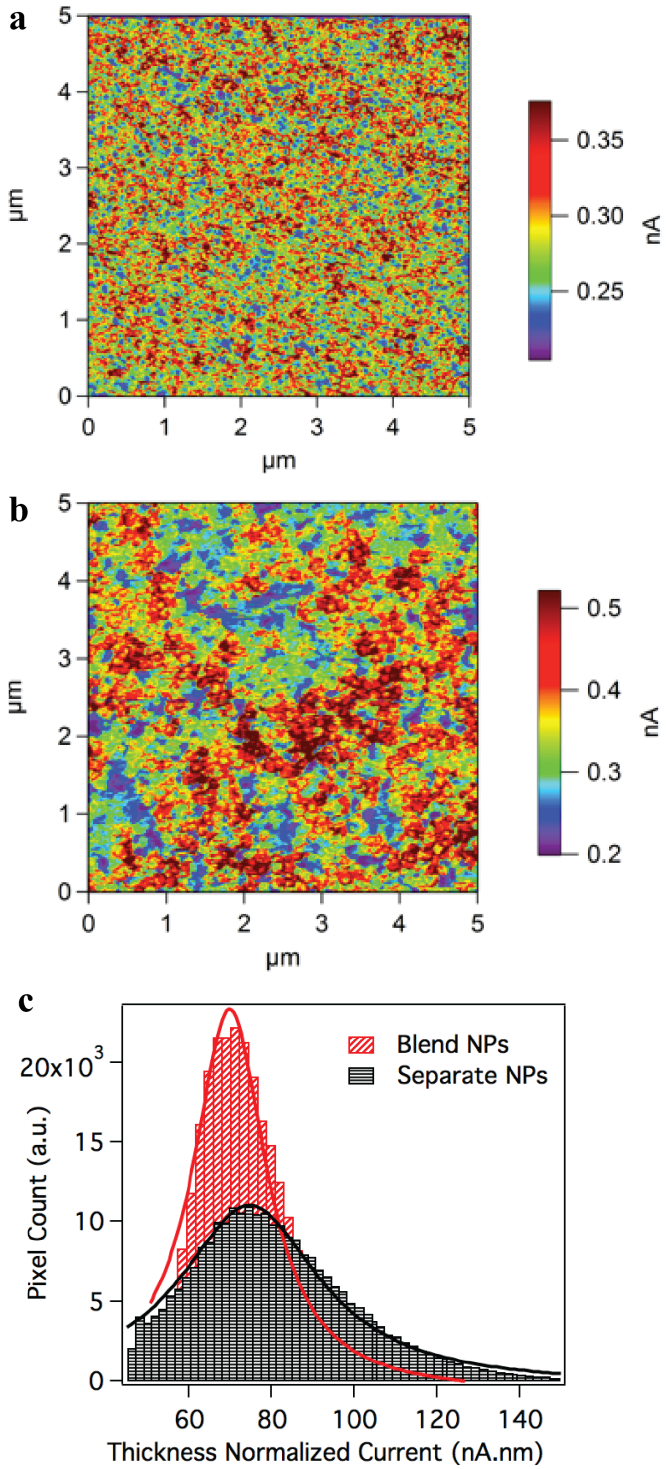

Figure 23: (a) cAFM Image of P3HT and PCBM Blend NPs (1:1 by wt. ratio.) Without a PCBM Top Layer. (b) cAFM Image of Separate P3HT NPs and PCBM NPs (1:1 by No. Ratio) Without a PCBM Top Layer. (c) Histogram Plot Depicting Normalized Pixel Count with Associated Currents Measured for Blend NPs, and for Separate NPs.

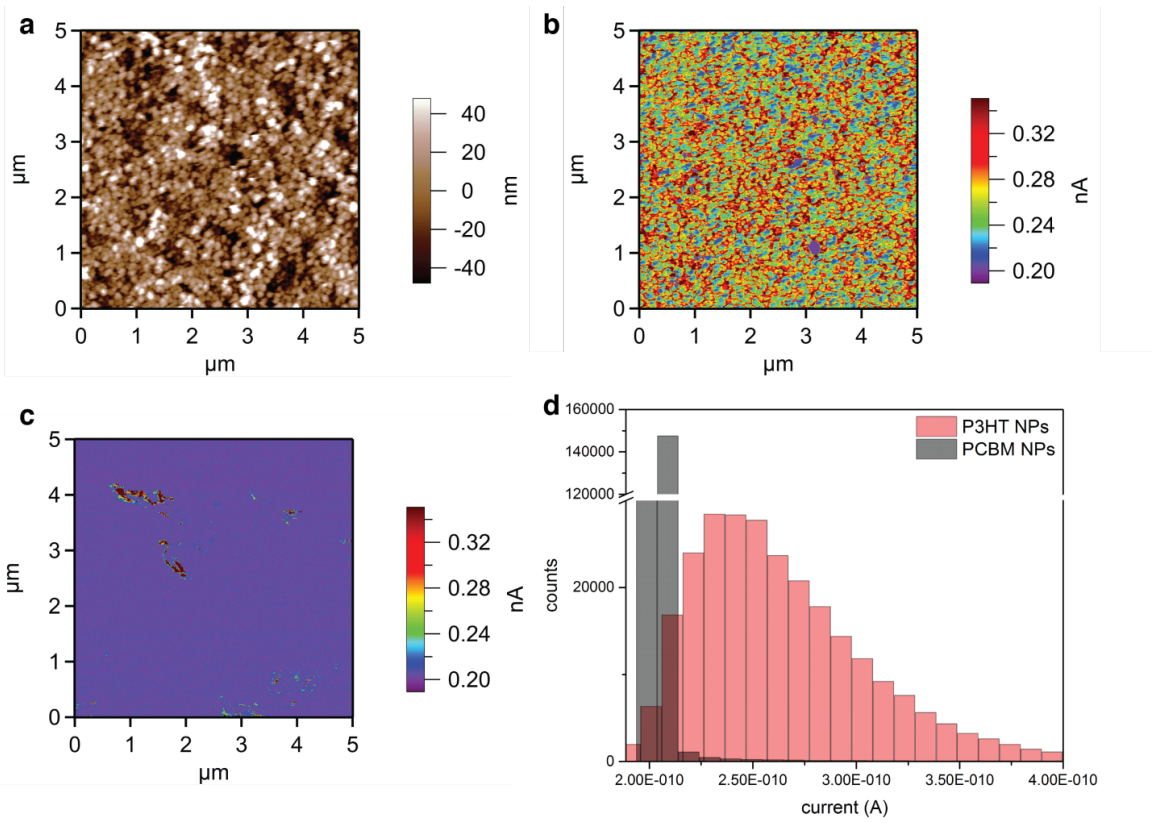

Figure 24: (a) Height AFM Image of P3HT Only Nanoparticle Film; (b) Corresponding cAFM Image of P3HT Only Nanoparticle Film in Image a; (c) c-AFM Image of a PCBM Only Nanoparticle Film Where a 2V Bias Voltage was Applied Between ITO Substrate and Conducting AFM Tip; (d) Current Mapping Histogram of the c-AFM Images in a and b.

Time of Flight (TOF) mobility measurements of P3HT, P3HT:PCBM blend, and P3HT and PCBM separate NP films were carried out to determine the effectiveness of their charge conduction pathways (Figure 25). P3HT NP films have a hole mobility of $\sim 2\times10^{-4}$ $cm^2V^{-1}s^{-1}$, the same order of magnitude as seen for pristine P3HT films. A 1:1 mixture of separate P3HT NPs and PCBM NPs shows a hole mobility of $\sim 8\times10^{-5}$ $cm^2V^{-1}s^{-1}$. In both cases, the mobility has only a weak field dependence. Blend NPs comprised of 1:1 weight:weight ratio of P3HT to PCBM has a hole mobility comparable to that for a P3HT-only NP film at a low-field regime, but the mobility decreases with increasing field. This behavior is attributed to positional

disorder in the Bässler model for charge transport in disordered solids.[75] The cAFM and TOF data indicate fundamental differences in the conductive pathways between blend and separate NP films.

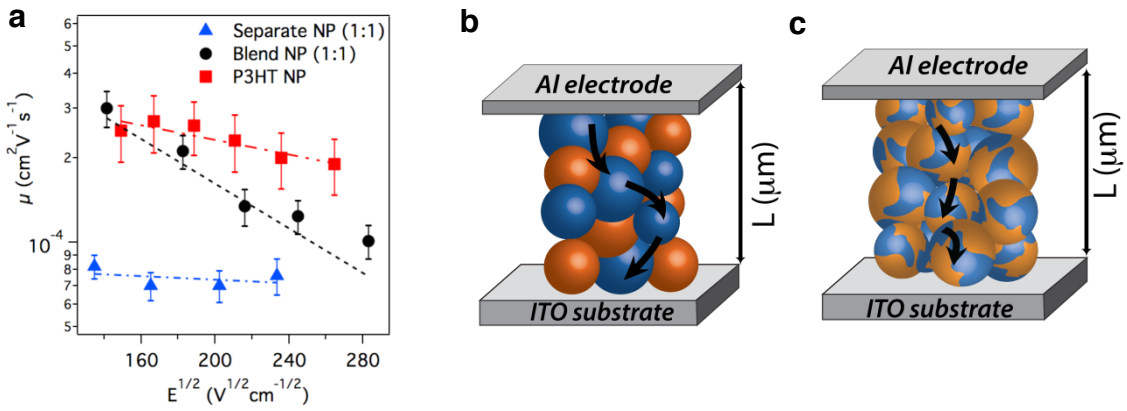

Figure 25: (a) Electric Field Dependent TOF Mobility of P3HT NPs, P3HT and PCBM Blend NPs and P3HT and PCBM Separate NPs Film. (b) Schematic Diagram of P3HT and PCBM Separate NPs Film Showing Hole Conduction Pathway. (c) Schematic Diagram of P3HT and PCBM Blend NP Film Showing Hole Conduction Pathways.

4.2.3 Nanoparticle Organic Photovoltaic Device Optimization and Preparation

This section includes an adapted excerpt from Bag, M.; Gehan, T.S.; Renna, L.A.; Algaier, D.D.; Lahti, P.M.; Venkataraman, D. Fabrication Conditions for Efficient Organic Photovoltaic Cells from Aqueous Dispersions of Nanoparticles. *RSC Adv.* **2014**, 4, 45325-45331 - Adapted with permission of The Royal Society of Chemistry

For fabricating OPV devices, aqueous dispersions of P3HT:PCBM blend NPs or separate NPs of P3HT and PCBM were spin coated onto ITO substrates coated with PEDOT:PSS, which acts as a hole transporting layer. Except for electrode deposition, these and all subsequent fabrication steps were done in ambient atmosphere. The PEDOT:PSS layer was treated with UV-O_3 for 3 min to increase surface hydrophilicity, which was found to be critical for achieving uniform films of

NP assemblies as seen in optical microscopy images. AFM analysis of surface roughness of NP films with a typical thickness of ~240 nm decreased from ~70 nm to ~10 nm for fabrication that included the UV-O_3 treatment. Immediately after UV-O_3 treatment, an aqueous dispersion of blend NPs or separate NPs was spin coated on top, under illumination by a commercial infrared (IR) lamp. After drying at room temperature in a vacuum chamber for 12 h, a thin layer of PCBM as an electron transporting layer (ETL) was spin coated from an orthogonal solvent (DCM) on top of the NP film, followed by vapor deposition of cathode (Ca/Al). Use of the ETL was critical for achieving a high fill factor in performance measurements of the final solar cells.

A cAFM image of a thin film of P3HT:PCBM blend NPs with a thin coating of PCBM on top is shown in Figure 26. The corresponding height image indicates that the PCBM top layer reduces surface roughness of the NP film by comparison to without the PCBM top layer, and Figure 26 indicates that the PCBM top layer blocks many pathways for holes to reach the top electrode, thus reducing leakage current. We found similar results for a thin film of co-assembled separate NPs with a PCBM top ETL. The best efficiency was achieved when the NP dispersion solvent was changed from water to 20% ethanol by volume in water. These dispersions led to the highest device performance for both blend (2.15%) and separate (1.84%) NPs; the current-voltage device performance curve is shown in Figure 32a.

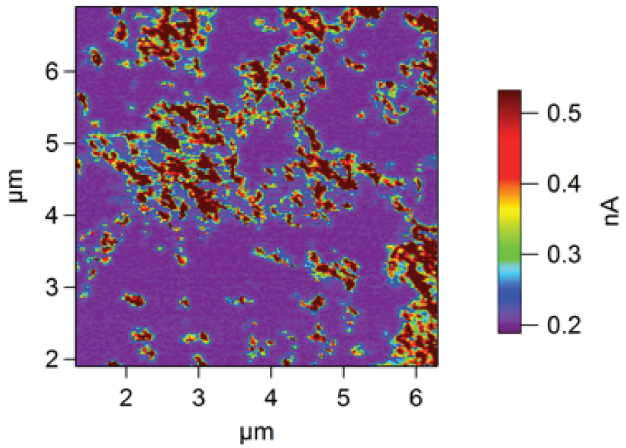

Figure 26: cAFM Image of P3HT:PCBM Blend NP-OPV Devices with PCBM Buffer Layer.

Devices were fabricated using these improved processing conditions, and show a significant enhancement in PCE from 0.46% to 2.15%. As seen in Figure 27 (see also in Table 1), the following necessary steps improve PCE from conditions used in processes P1 to P6, as listed below:

Process P1: Nanoparticle active layer was spin coated onto "as prepared" PEDOT:PSS layer. Ca/Al electrode was thermally deposited on top.

Process P2: Active layer was spin coated on UV-O_3 treated PEDOT:PSS layer. Ca/Al electrode was thermally deposited on top.

Process P3: Active layer was spin coated onto "as prepared" PEDOT:PSS layer. A thin PCBM buffer layer was spin coated on top from a 15 mg/mL concentration in dichloromethane solution at 1000 rpm speed for 40 s, followed by Ca/Al electrode deposition.

Process P4: Active layer was spin coated onto UV-O_3 treated PEDOT:PSS substrate. A thin PCBM ETL was spin coated on top from a 15 mg/mL in dichloromethane concentration solution, followed by Ca/Al electrode deposition.

Process P5: Active layer was spin coated onto UV-O_3 treated PEDOT:PSS substrate. Active layer was then washed with 50% ethanol in water before the PCBM ETL was coated on top, followed by Ca/Al electrode deposition.

Process P6: 20% ethanol in water was added to nanoparticle dispersion before final centrifugal filtration. Active layer was then spin coated onto UV-O_3 treated PEDOT:PSS substrate. A thin PCBM ETL was then spin coated on top, followed by Ca/Al electrode deposition.

Except for the electrode evaporation step, the devices were fabricated in ambient atmosphere. We have also fabricated devices from separate P3HT and PCBM nanoparticles to prove the generality and reproducibility of the method with a success rate over 80%, based on power conversion efficiency (PCE) measurements from the final devices.

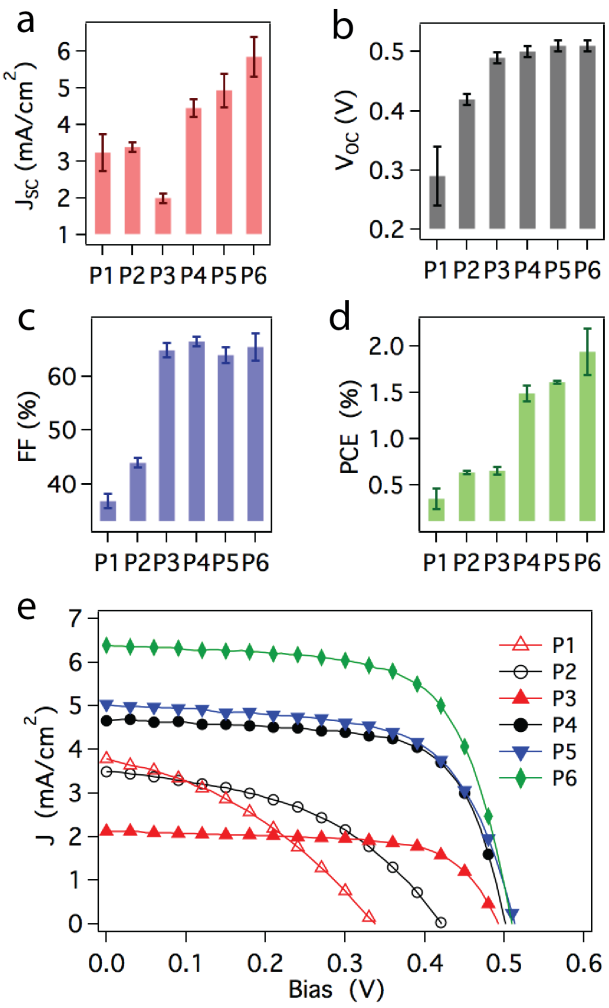

Figure 27: (a-d) P3HT:PCBM Blend Nanoparticle Device Performance Under Different Processing Conditions. (e) Current-voltage Performance of the Devices Under AM 1.5G Solar Simulator at 100 mW/cm² Light Intensity

Table 1: Performance of P3HT:PCBM Blend Nanoparticles Devices Fabricated from Different Processing Conditions. Best Obtained Values are Given in Parentheses.

Processing conditions	J_{SC} (max) (mA/cm^2)	V_{OC} (max) (V)	FF (max) (%)	PCE (max) (%)	R_s (typical) (Ω cm^2)	R_{sh} (typical) (kΩ cm^2)
P1	3.25 (3.75)	0.29 (0.34)	36.8 (38.2)	0.35 (0.46)	47.5	0.29
P2	3.40 (3.52)	0.42 (0.43)	43.9 (44.8)	0.64 (0.66)	39.5	0.47
P3	2.0 (2.12)	0.49 (0.50)	64.8 (66.2)	0.65 (0.69)	24.0	2.50
P4	4.46 (4.69)	0.50 (0.51)	66.5 (67.4)	1.49 (1.58)	11.4	1.50
P5	4.94 (5.40)	0.51 (0.52)	64.0 (66.5)	1.61 (1.63)	13.8	1.51
P6	5.84 (6.38)	0.51 (0.52)	65.4 (67.9)	1.94 (2.15)	9.78	1.45

4.2.3.1 Impact of Post-Heat Treatment on Device Performance

Unlike in conventional solution film coating fabrication, in nanoparticle film coatings P3HT is in a semicrystalline aggregated structure *prior* to thin film formation. Therefore, one expects that thermal annealing should have minimal impact on the polymer crystallinity and hence the device PCE. In fact, in one literature example, thermal annealing gave PCE *decreases* for P3HT:PCBM blend nanoparticle solar cells.[76] But, our results indicate that controlled heat treatment (post-heating) is required for optimum device performance using our fabrication protocol. Figure 28a through Figure 28d show device performance as a function of post fabrication heating temperatures. In all the measurements, substrates were slowly heated from 30 °C to the final temperature with a heating rate of 5 – 10

°C/min. Significant improvement in the V_{OC} as well as the FF was observed when the devices were heated up to 80 °C, which is well below the P3HT crystal re-orientation temperature ($T_m \sim 195$ °C) reported in the literature.[77] We surmise that the slow heating of the substrate improves the interfacial interactions between polymer nanoparticles, and the interlayer interactions between nanoparticles and electrodes.[8] The J_{SC} was increased only when devices were heated above 110 °C. This could be due to PCBM cold crystallization which occurs in the temperature range of 103 – 119 °C for P3HT:PCBM blends of 1:1 by weight ratio.[77] P3HT crystallinity does not change upon heating to 150 °C in x-ray diffraction measurements (see Figure 29), although a strong crystalline peak from PCBM grows after heating at 150°C. P3HT and PCBM are miscible, such that only one glass transition temperature (T_g) is observed for any binary composition between these. Thus, any structural changes presumably happen during nanoparticle synthesis at a 70 °C, since T_g for the 1:1 P3HT:PCBM blend is less than 40 °C.[78,79] However it should be noted that prolonged heating of these devices after fabrication results in decreased efficiency.

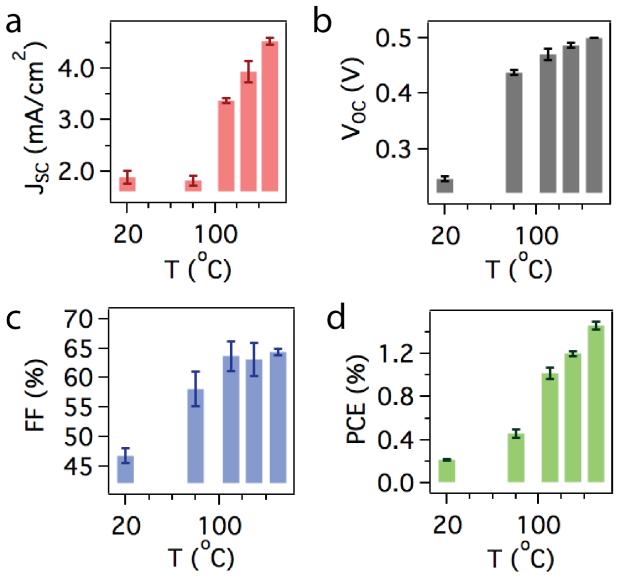

Figure 28: P3HT:PCBM Blend Nanoparticle Devices Performance at Different Annealing Temperatures

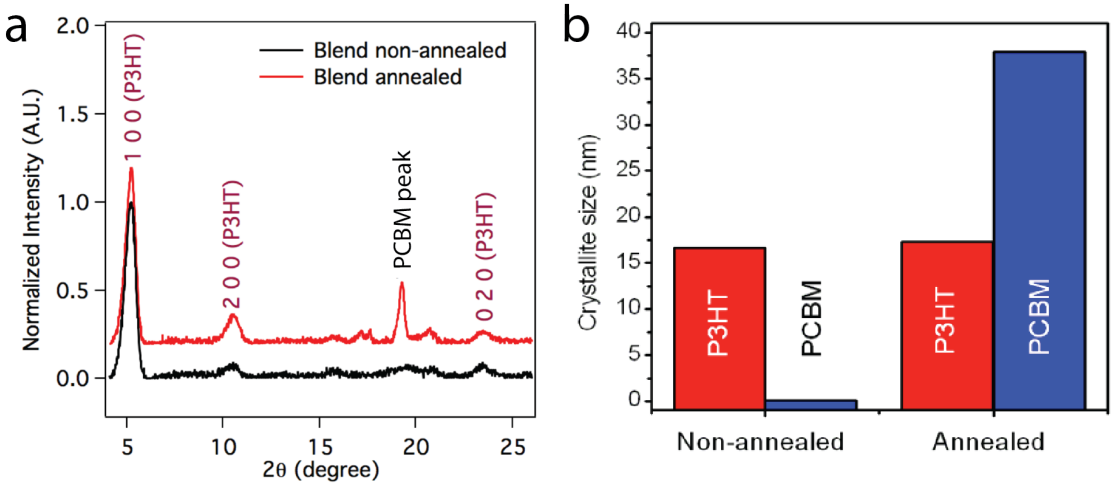

Figure 29: (a) XRD of P3HT:PCBM Blend Nanoparticles Drop-Cast on Glass Substrates and Dried Under IR Lamp. Annealed Sample was Slowly Heated from 30 °C to 150 °C. (b) Crystallite Size Estimated from the XRD Peak Width.

4.2.3.2 Light Intensity Dependence Study: Structure-Property Correlations

To understand further the device performance parameters obtained for the P3HT/PCBM nanoparticle solar cells, we carried out incident light intensity dependence measurements of I-V performance on a blend nanoparticle device with PCE ~2.0%. These are shown in Figure 30a. The observed high FF – over 67% even

at 100 mW/cm^2 light intensity – indicates a balanced transport of electron and holes to their respective electrodes and with limited bimolecular recombination losses. A linear increase in J_{SC} with increasing light intensity was observed, as shown in the Figure 30b. However, a slight drop in efficiency occurred as light intensity was decreased, mainly due to a drop in V_{OC}.

The cAFM measurements are a useful tool to probe the active layer morphology and how it relates to charge transport through the device active layer. The cAFM image in Figure 31a indicates that the PCBM buffer layer (ETL) not only reduces the surface roughness (~10 nm), but also prevents undesired leakage hole transport to the top (cathode) electrode (Figure 31c). Hence a significant improvement in FF and V_{OC} is observed in devices using this buffer, blocking layer. Upon washing devices with dichloromethane (DCM), this PCBM buffer layer was removed and the cAFM shows that uniform conduction pathways remain for holes (Figure 31d), which is in good agreement with the high J_{SC} observed in these devices. A quantitative analysis of conduction pathways with (Figure 31a) and without (Figure 31d) the PCBM buffer layer as shown in Figure 31f, is in good agreement with low leakage current and high FF observed in devices with a PCBM buffer layer. There is still some scope for improvements if we can reduce the non-uniformity in the PCBM buffer layer thickness as seen in Figure 31b and Figure 31c.

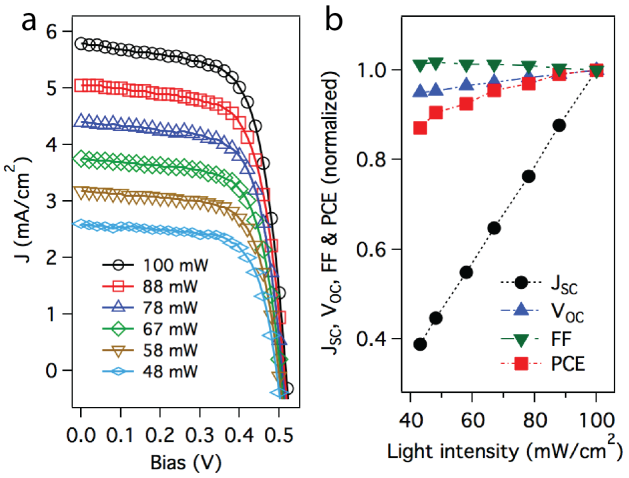

Figure 30: (a) Light Intensity Dependent I-V Curve of a P3HT:PCBM Blend Nanoparticle Device; (b) Device Parameters Normalized with Respect to 100 mW/cm² as a Function of Light Intensity.

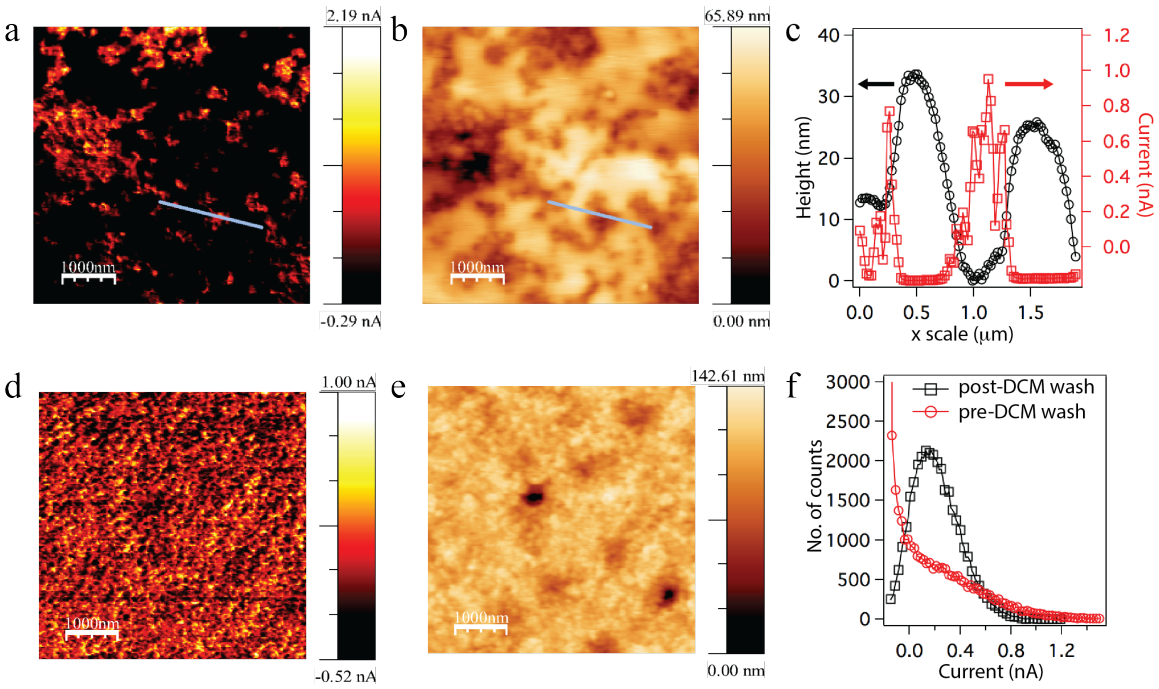

Figure 31: (a) cAFM Image of P3HT/PCBM Blend Nanoparticle Device with PCBM Buffer Layer on Top; (b) AFM Topographic Image of the Same Region; (c) Line Profile of AFM Height and Current Contrast Image Showing PCBM Layer Reduces Leakage Current; (d) cAFM Image of the Same Film After Washing with DCM; (e) AFM Height Image of the Same Region as Mentioned in d; (f) Current Distribution Plot (Number of Pixels with Particular Current Value Measured by AFM Probe Tip Under Applied Bias Condition) of Nanoparticles Device with PCBM Buffer Layer (Pre-DCM Wash Shown in a, and Post-DCM Wash Shown in b).

4.2.4 Systematic Tuning of Nanoparticle Domain Size and Morphology

The power of using sphere packing for OPV applications is the ability to independently tune the domain size while keeping the morphology constant and vice versa, which thus far has been elusive. To probe the effect of domain size on OPV performance, devices from separate and blend NPs were prepared using nominal particle mode diameters of 115 nm, 90 nm, 80 nm, and 70 nm. The concentration of P3HT to PCBM was held constant (1:1 weight ratio) for the devices prepared with either blend or separate NPs. The expectation for blend NPs is that

the domain size for each component is similar for *all* particle sizes; therefore particle size should have a minimal impact on efficiency. The expectation for separate NPs is that the efficiency will increase with decreasing particle size until the size approaches the exciton diffusion length.

Four sets of devices were prepared, keeping the sizes of P3HT and PCBM separate NPs the same within each set. The impact of particle size on power conversion efficiency (PCE) for blend and separate NPs is shown in Figure 32b. Contrary to expectation, both blend and separate NP devices showed optimal performance at a domain size of 80 nm. This supports the recently increasing belief that optimal domain size for organic solar cells can be larger than 10 nm.[80]

To probe the impact of morphology with constant domain size, OPV devices were fabricated by changing the ratio of the number of p-type (P3HT) domains to the number of n-type (PCBM) domains. Upon increasing the ratio of P3HT NPs to PCBM NPs from 1:1 to 4:1 the PCE drops from 1.78% to 1.38%, as seen in Figure 32c. The most efficient ratio of P3HT to PCBM NPs was 2:1 with a maximum efficiency of 1.84%. By controlling the relative ratio of separate NPs, we can control the morphology of the active layer. The cAFM images of 1:1 and 2:1 P3HT NPs to PCBM NPs (Figure 33a and Figure 33b respectively) indicates that the morphologies are different. As the ratio of P3HT NPs to PCBM NPs increases (from 1:1 to 2:1 to 1:0, Figure 33a-Figure 33c), the number of hole conducting pathways also increases, leading to increased current. This increase in current is clearly seen in in Figure 33d. This method provides a potentially general approach that would enable the

independent optimization of the domain size and morphology for enhanced device performance.

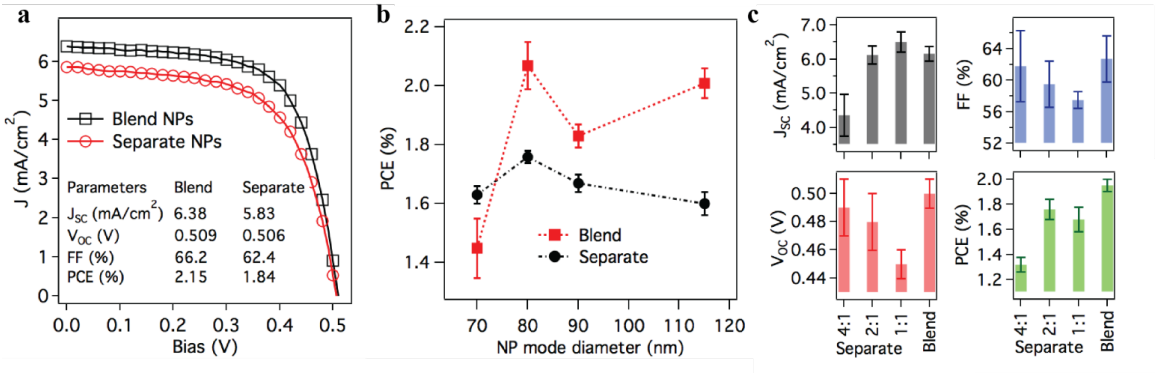

Figure 32: (a) NP OPV Device Performance of P3HT:PCBM Blend (1:1 Weight Ratio) NPs, and P3HT and PCBM Separate (2:1 Number Ratio) NPs; (b) P3HT and PCBM Separate (1:1 Number Ratio) NPs Size Dependent PCE, and P3HT:PCBM Blend (1:1 Weight ratio) NPs Size Dependent PCE; (c) Device Performance of P3HT and PCBM Blend and Separate NPs Devices at Different Ratio of P3HT NP to PCBM NP. All Particles are ~ 80 nm (Mode Diameter).

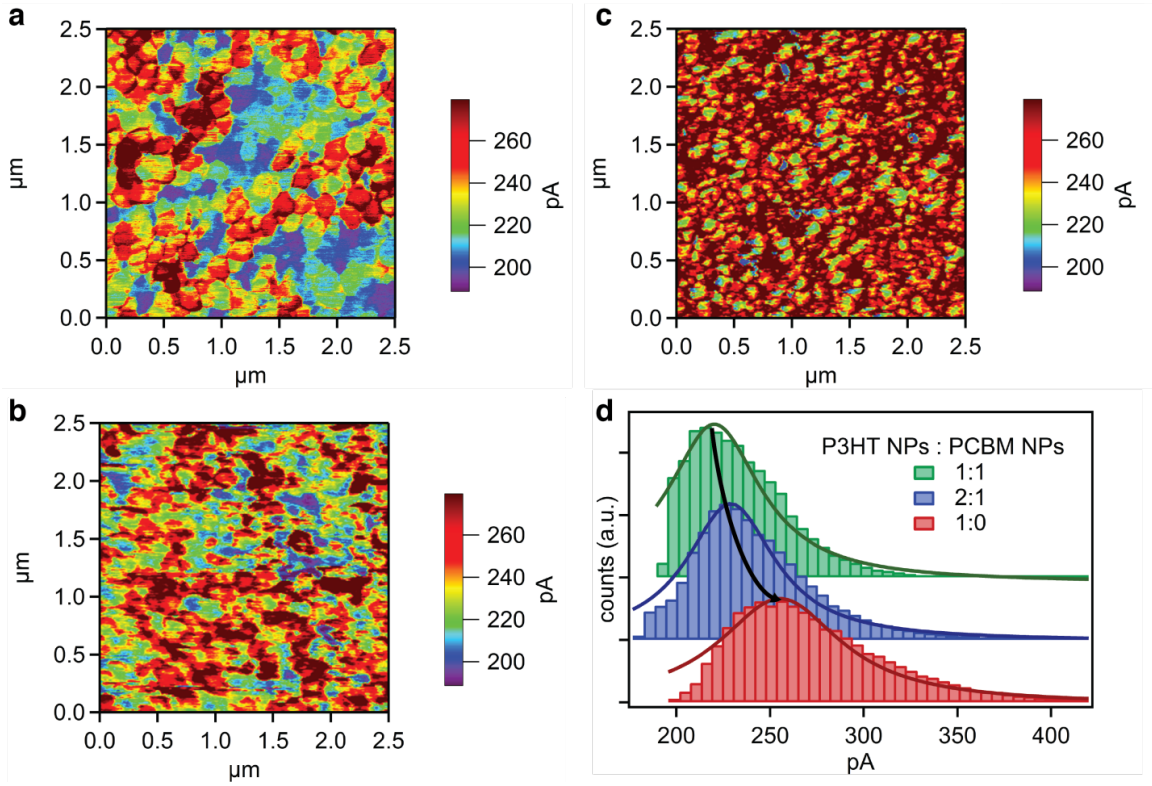

Figure 33: (a) cAFM Image of a 1:1 Number Ratio of P3HT NPs to PCBM NPs Without a PCBM Top Layer; (b) cAFM Image of a 2:1 Number Ratio of P3HT NPs to PCBM NPs Without a PCBM Hole-Blocking Top Layer; (c) cAFM Image of Only P3HT NPs (1:0 Number Ratio) Without a PCBM Top Layer; (d) Histogram Plot Depicting the Pixel Count with Associated Currents Measured for the cAFM Images in a, b, and c.

In the DV group, we have used the concept of sphere packing to control the hierarchical active layer morphology of OPV cells by pre-formed each active layer component as nanospheres and fabricating uniform nanosphere assemblies. In contrast to conventional methods of controlling active layer morphologies, this approach affords the ability to (a) pre-tailor the semiconductor domains with the required internal packing and size; (b) obtain stable co-continuous structures that are controlled from the nanoscale to mesoscale, through self-assembly into equilibrium or kinetically-trapped morphologies in a single step; (c) use multiple hole conductors to broaden the absorption spectrum; (d) systematically elucidate

the optimal structure for an efficient OPVs and (e) use environmentally benign solvents such as water for device fabrication. Controlling each active layer component at multiple length scales using sphere packing not only offers a method for developing next generation OPVs, but also opens a revolutionary pathway for the systematic study and tuning of functional materials while exercising control of the component assembly at multiple length scales.

It should be noted that the simulated random assembly of spheres, conducting AFM measurements, and XRD were done by Lawrence Renna (Venkataraman "DV" Group). The OPV device preparation, device characterization, and TOF measurements were performed by Dr. Monojit Bag (Venkataraman "DV" Group). Some of the SEM images were prepared by Xiaobo Shen (Russell Group in the Polymer Science and Engineering Department) and some were prepared by Dana D. Algaier (Venkataraman "DV" Group). I carried out all the nanoparticle syntheses, their purification, and characterization for all samples. Experimental design was performed by all the authors in the paper.

CHAPTER 5

FUTURE DIRECTIONS AND PROJECT OUTLOOK

5.1 Future Directions

There is a significant amount of research in the area of organic photovoltaics on trying to understand how to control electroactive molecule/polymer packing within the active layer. The problem with traditional methods to try and control the morphology are completely dependent on intermolecular interactions: donor:donor, donor:acceptor, and acceptor:acceptor. There are techniques and "tricks" to try to tune the intermolecular interactions, like using an additive with selective solubility for one component. But, it is extremely difficult to tune morphology systematically in a way to allow consistent and predictable variation of the electronic properties by creating specific morphologies within the active layer.

Throughout this dissertation I have outlined a method to tune the morphology systematically from the molecular scale through the mesoscale of organic photovoltaic devices, by using organic nanoparticles, without being completely dependent on intermolecular interactions between donor and acceptor materials. Some of the key findings include: 1) nanoparticle diameter and size distribution can be tuned by changing the polymer concentration and surfactant concentration; 2) charges can be efficiently transported through assemblies of semiconducting polymer nanoparticles prepared from an aqueous solution containing electrically insulating surfactants; 3) organic photovoltaic devices can be prepared with an active layer, processed from an aqueous solution, consisting of a

"random" binary assembly of organic nanoparticles with efficiencies comparable to a bulk-film coated BHJ using the same active layer materials; 4) internal active layer morphology can be systematically tuned for organic nanoparticle photovoltaic devices by changing the average nanoparticle size and the number ratio of donor to acceptor nanoparticles; 5) The optimum nanoparticle size for device performance was ~80 nm P3HT nanoparticles mixed with ~80 nm PCBM nanoparticles. This contradicts the initial notion that the nanosized donor (P3HT) rich and acceptor (PCBM) rich domains must be around 20 nm. Also effective devices were prepared using separate nanoparticles of P3HT and PCBM with a mode diameter of ~115 nm, which is counterintuitive with the exciton diffusion limited model for charge extraction.

The findings were made using P3HT and PCBM as the donating and accepting materials, but this approach should theoretically be very versatile for any combination of donor and acceptor to be used with control of molecular scale to mesoscale packing. To prove this, the approach must be demonstrated with other electronically proven donating and accepting materials. PCPDTBT/PCBM and PTB7/PCBM hole/electron pairings would be ideal device active layer materials to demonstrate the versatility of the organic nanoparticle method for active layer morphology control because there has been a lot of work on understanding the morphologies of these active layer materials, as described in chapter 1. Use of this approach would offer, for the first time, the prospect to systematically tune the domain size of each active layer material and determine by rational variation what active layer morphology results in optimum device performances.

Although it would be exceedingly difficult to prepare on a large commercial scale, it would be extremely beneficial scientifically to prepare crystalline superlattices of donor nanoparticles with acceptor nanoparticles. By changing the crystalline lattice one could (in principle) tune the packing of the donor and acceptor materials with utmost control. Therefore, the optimum morphology could be unequivocally determined because of the high level of control over morphology.

But, the present methodology now allows individual tuning of the molecular packing, of nanosized domains, or of the mesoscale packing of the nano domains, each without affecting the other scale organization. Therefore, directly correlation becomes possible for each of these to electronic properties and overall device performance, which is impossible by the current, highly coupled methods for preparing active layer hierarchical assemblies. Essentially this method gives the control required to probe the morphology systematically within binary blends of polymers/molecules.

As difficult as it is to control the morphology in binary blends of organic polymers/molecules, as a community we know even fewer methods to predict/control morphology within ternary blends. The method outlined in this dissertation could be used to control the morphology within ternary blends of active layer materials by use of three different nanoparticle solutions. Theoretically, by mixing multiple nanoparticle solutions as active layer materials, a wide range of the visible spectrum could be absorbed, while achieving energy level match up to allow charge transport between p-type and n-type materials. The nanoparticle method for preparing the active layer in organic photovoltaics offers control over active

material organization on multiple length scales that current methods just cannot offer.

The organic nanoparticle photovoltaic devices in this work were prepared with a device area of 6 mm^2, which is acceptable as a proof of concept. If this device architecture is to ever be commercialized, then efficient devices will have to be prepared as much larger scale prototypes. For this architecture to be scaled up, the processing for each layer has to accommodate a roll-to-roll or similar processing method. For example, ITO coated polyethylene terephthalate (PET) can be purchased as large area rolls. The processing of PEDOT:PSS has already been demonstrated by multiple roll-roll-methods.[81] The key steps to advance from this point will be determining how to scale up the processing of an organic nanoparticle active layer from an aqueous dispersion, and how to process the electron transporting interlayer (PCBM interlayer). It would be desirable to find an electron transporting interlayer that is processable as an aqueous solution. One of the biggest problems with scaling up organic photovoltaic materials has been controlling the morphology within large-scale devices. The organic nanoparticle method could solve this problem, since the nanomorphology during the nanoparticle synthesis and control of large-scale morphology will be solely dependent on the packing of spheres as large area films.

There are many applications that use binary blends of polymers/organic materials, although I have only shown one application, organic photovoltaics, for this dissertation. Thermoelectric materials create an electrical current from a gradient in temperatures. Organic thermoelectric materials could benefit from

controlling the assembly of two polymeric materials at multiple length scales to tune the thermal and electrical conductivities and thus the device performance.[82] This exemplifies one of many applications that could be enhanced and systematically tuned by using the methods developed in this dissertation.

CHAPTER 6

EXPERIMENTAL

Bag, M.; Gehan, T.S.; Renna, L.A.; Algaier, D.D.; Lahti, P.M.; Venkataraman, D. Fabrication Conditions for Efficient Organic Photovoltaic Cells from Aqueous Dispersions of Nanoparticles. *RSC Adv.* **2014**, 4, 45325-45331 – Reproducedwith permission of The Royal Society of Chemistry
[Some changes to the published text were made for adapted use in this dissertation.]

6.1 Generalized Conjugated Polymer Nanoparticle Synthesis Using the Miniemulsion Method

Commercially available poly(3-hexylthiophene) (P3HT) from Rieke Specialty Polymers with molecular weight 36 kDa, 96% regioregularity, and Đ = 2.3 was used without further purification. $PC_{61}BM$ from Nano-C was used as received. Sodium dodecylsulfate (SDS, 98% purity) from Sigma Aldrich was used. Thermo Scientific Barnstead Nanopure water was used. Vivaspin 6 centrifugal filter tubes 10 kDa MWCO PES (molecular weight cutoff polyether sulfone) membrane was obtained from Vivaproducts. A Misonix Sonicator 3000 ultrasonicator with a 1/8" probe tip from Qsonica was used to prepare the miniemulsions. A VWR Scientific Products Model 50T Aquasonic bath sonicator was used for initial solution preparation.

Organic semiconductor nanoparticle dispersions were prepared using a modified miniemulsion method that requires the preparation of two solutions: a polymer in oil (chloroform) solution, and an aqueous surfactant solution. For blend nanoparticles both P3HT and PCBM were dissolved in chloroform, and for separate component nanoparticles either P3HT or PCBM was dissolved in chloroform. For blend nanoparticles, typically a 30 mg/mL (total, varying ratio of components) of P3HT and PCBM solution in chloroform was heated at 35˚C for at least 30 min with

continuous stirring to ensure dissolution. A 10 mM SDS solution was separately prepared with nanopure water. To ensure dissolution of the SDS, the solution was heated gently with a heat gun and sonicated in a bath sonicator for a minute. Next, 3.0 mL of the 10 mM SDS solution was added to a 15 mL centrifuge tube, followed by 0.3 mL of the 30 mg/mL organic semiconductor in chloroform solution. The centrifuge tube was immediately lowered into an ice bath, a 1/8" sonicator probe tip was lowered approximately half way into the solution, and the mixture was ultrasonicated at 20% max amplitude for 2 min. Immediately after sonication, the emulsion solution was poured into a 20mL cylindrical glass vial and heated in an aluminum block, set at 70˚C, for 40 min with continuous stirring by a small stir bar. The nanoparticle dispersion was then allowed to cool to room temperature while open to bench top atmospheric conditions. A second solution was then prepared in the same manner. Then both nanoparticle dispersions were placed in a single Vivaspin 6 centrifugal filter tube. The tube was centrifuged at 4180 relative centrifugal force (rcf) for 25 min. The filtrate was removed and the retentate was diluted to 5 mL with nanopure water. The centrifugation process was repeated three more times. For the final (5th) centrifugal filtration cycle, the retentate was diluted with 20 vol% ethanol in water and then centrifuged at 4180 rcf for 45 min. The retentate was then diluted to 0.5 mL with 20 vol% ethanol in water. This solution was then used as is, and immediately spin-coated onto device substrates.

6.1.1 Tunability Within the Nanoparticle Synthesis Method

The size of conjugated polymer nanoparticles can be tuned by changing multiple parameters: surfactant type and/or concentration, polymer concentration, oil layer composition (solvent choice, concentrations), aqueous layer composition, and by sonication parameters (vessel shape, sonication time, sonication intensity, continuous vs. pulsed sonication). As the polymer concentration is increased, generally the polymer nanoparticle size increases. Changing the polymer concentration can additionally change oil layer solution properties (e.g., surface tension and viscosity), which will affect the droplet size in the miniemulsion and thus affect the polymer nanoparticle size. As the surfactant concentration increases, generally the nanoparticle size decreases rapidly. Changing the aqueous layer to a water/alcohol mixture also can be used to tune the nanoparticle size. When using SDS as surfactant, a mixture up to 20% ethanol in water can be used to prepare P3HT nanoparticles from a P3HT in chloroform oil layer. Although this has not been thoroughly studied, the oil layer solvent apparently can be changed, as long as it is not soluble in water. The following oil layers have been used to successfully prepare P3HT nanoparticles: chloroform, chlorobenzene, toluene, and xylene. The sonication parameters (sonication power, sonication time, sonicator tip size) can be used to tune the nanoparticle size, but the focus when changing the sonication parameters should be to achieve consistency of the emulsion droplet size.

6.2 Organic Nanoparticle Photovoltaic Device Preparation and Testing

All photovoltaic performance, electrical, and charge mobility measurements were carried out at PHaSE-EFRC Photovoltaic Facility at the University of Massachusetts, Amherst. I am grateful for major assistance with these measurements from Dr. Monojit Bag of the DV group, and Prof. Volodimyr Duzhko, the Facility Director.

Commercially available ITO substrates (TFD Inc, ~20 Ω/cm^2) were cleaned by ultra-sonication in soap solution (Versa Clean, Fisherbrand) and distilled water, then with acetone, followed by isopropyl alcohol. They were then kept in hot air oven at 140 °C for 2 h, following which they were treated with UV-O_3 for 15 min (UVO cleaner, Jelight Company, Inc). Poly(3,4-ethylenedioxythiophene):polystyrene sulfonate (PEDOT:PSS) (Clevios P VP AI 4083, in water used as received) was spin coated on the substrate at 2500 rpm for 30 s after filtration through a 0.45 micron PVDF filter (Wilkem Scientific). The PEDOT:PSS coated substrates were then annealed at 150 °C for 20 min in air, and allowed to cool to room temperature. For some preparations, the substrate at this point was again exposed to UV-O_3 for 3 min. Polymer nanoparticles of P3HT and PCBM that were synthesized as described above were then used to spin coat active layers at 1000 rpm for 60 s onto PEDOT:PSS-coated ITO substrates. Again, this step can be followed or not by UV-O_3 treatment of PEDOT:PSS, depending on the preparation. Any PEDOT:PSS layer without UV-O_3 treatment will be described “as prepared” PEDOT:PSS.

A small humidifier was used to control the humidity of the spin-coating deposition chamber, with the best device power conversion results obtained for

30% chamber humidity. For some experiments, PEDOT:PSS coated substrates were pre-heated with an infrared lamp before or during nanoparticle active layer coating. ITO/PEDOT:PSS/(nanoparticle) samples were then kept in a vacuum chamber for 10-12 h to remove excess water content in the films. For some samples, a thin layer of $PC_{61}BM$ from 15 mg/mL in dichloromethane solution was spin coated atop the nanoparticle layer, at 1000 rpm for 40 s. Next, a 15 nm thick Ca electrode was thermally deposited at a rate of 0.5 Å/s, overlaid next by a 100 nm Al electrode deposited at a rate of 1 – 3 Å/s at a chamber pressure of 1×10-6 mbar. Devices were then annealed by slowly heating in a glove box under nitrogen from room temperature to specific temperatures described for individual experiments (using a hotplate), then removed from the hot plate and immediately subjected to solar conversion performance measurements. An AM1.5G solar simulator was used for device characterization with a light intensity of 100 mW/cm2; the source was periodically calibrated by Prof. V. Duzhko to maintain appropriate intensity.

6.3 Nanoparticle Sample Preparation for Time-of-Flight (TOF) Charge Mobility Measurements

The time of flight devices were prepared differently in chapter 3 and chapter 4. Therefore, two separate procedures are listed below.

6.3.1 Sample Preparation of TOF Devices from Chapter 3

Adapted with permission from Bag, M., Gehan, T. S., Algaier, D. D., Liu, F., Nagarjuna, G., Lahti, P. M., Russell, T. P. and Venkataraman, D. Efficient Charge Transport in Assemblies of Surfactant-Stabilized Semiconducting Nanoparticles. Adv. Mater. 2013 25: 6411–6415. doi: 10.1002/adma.201301302 Copyright John Wiley and Sons.

http://onlinelibrary.wiley.com.silk.library.umass.edu/wol1/doi/10.1002/adma.201301302/full

(Some changes to the published text were made for adapted use in this dissertation.)

P3HT nanoparticle dispersions were fabricated using a modified version of the above-described procedure with 5 mg/mL of P3HT in chloroform and 1 mM or 16 mM SDS solutions in nanopure water. As per the above procedure, after the nanoparticle dispersions were removed from the heat blocks and allowed to cool, the nanoparticle dispersions were transferred to a centrifugal concentrator tube and centrifuged at 4185 rcf for ~10 min per mL of nanoparticle dispersion. The retained dispersion was diluted with water and centrifuged again. A small drop of the filtrate was added to $BaCl_2$ (aq) to see if a precipitate formed, which would indicate remaining free surfactant. It was determined that excess surfactant was removed in two centrifugal filtration cycles, following which the dispersions were diluted with water such that the effective volume of the dispersion was half that of the original volume before centrifugation.

This conjugated polymer miniemulsion nanoparticle synthesis method was used to prepare the nanoparticles in the Advanced Materials paper cited for this subsection. The more detailed synthetic method was not further optimized at that time. Also, cylindrical vials were used as the sonication vessel, instead of centrifuge tubes.

ITO glass substrates (TFD Inc, 20±0.2 Ω/sq.) were cleaned by sonication in soap water solution (Versa Clean, Fisherbrand) for 30 min, followed by sonication in distilled water and then in isopropyl alcohol, each for 30 min. The substrates were then dried in air using a heat gun.

The pristine P3HT thin films were drop-cast from hot chlorobenzene solution (typically around 20 mg/mL) onto the cleaned ITO substrates, then annealed at 150 ˚C for 5 min inside a glove box (MBraun) under nitrogen. Nanoparticle films were prepared from both non-centrifuged nanoparticle dispersions and from centrifuged nanoparticle dispersions. The non-centrifuged nanoparticle dispersions did not undergo the previously described centrifugal filtration process and were used "as is" after they were heated on the heating block and allowed to cool. To prepare the nanoparticle film, typically 5 – 7.5 mL of the non-centrifuged nanoparticle solution was spray-coated at 15 psi nitrogen gas pressure from an Omni 5000 airbrush onto a cleaned ITO substrate placed on a hotplate set at 80-85 ˚C. Typically 3 – 4 mL of the centrifuged nanoparticle solution (because they are more concentrated) was spray-coated onto a clean, UV-O_3 treated ITO substrate. The fabricated substrates were placed in a vacuum desiccator at ~200 mTorr overnight at room temperature. A thin aluminum (Al) film of ~30 nm was then thermally deposited at 2×10^{-6} mbar. Time-of-flight (TOF) measurements were then carried out using a 355 nm pulsed laser (Continuum) illumination with a ~10 ns pulse lifetime through the semi-transparent Al electrode. The transient photocurrent at constant temperature (Instec MK1000 temperature controller, typically room temperature) was measured across 50 Ω to 5 kΩ resistances depending on the individual device. A variable DC voltage source (Agilent E3620A/E3612A) was used to apply a positive bias at the Al electrode with respect to the ITO electrode, and the resulting photoconduction signal recorded using a Tektronix TDS 3052C GHz oscilloscope. Nanoparticle film thicknesses were measured using an Alpha Step IQ profilometer after all electrical

measurements were completed. A film thickness of greater than 1 μm for TOF measurements is typically desirable.

6.3.2 Sample Preparation of TOF Devices from Chapter 4

Adapted with permission from Gehan, T.S.; Bag, M.; Renna, L.A.; Shen, X.; Algaier. D.D.; Lahti, P.M.; Russell, T.P.; Venkataraman, D. *Nano Letters* **2014** 14 (9), 5238-5243. Copyright 2014 American Chemical Society.

(Some changes to the published text were made for adapted use in this dissertation.)

TOF mobility measurement was carried out using P3HT spin-coated films (only), P3HT and PCBM separate, and P3HT:PCBM blend NP samples. The nanoparticle samples were prepared using the procedure described above in section 6.1. Films prepared from concentrated solutions of the nanoparticle dispersions were spin coated slowly (600 rpm) on UV-O_3 treated, pre-cleaned ITO substrates in the presence of infrared (IR) illumination. Film thickness was typically of 1 to 2 micrometer measured using an Alpha Step IQ profilometer. A thin layer (30 nm) of Al electrode was thermally deposited to illuminate through the electrode. 355 nm (Continuum) laser pulse (10 ns) was used to create sufficient amount of photo-generated carriers. Carrier drift current due applied electric field was then measured at variable DC bias voltages (Agilent E3620A/E3612A) across 500 ohm resistance connected in series with the device using GHz oscilloscope (Tektronix TDS 3052C).

BIBLIOGRAPHY

(1) Das, R.; Harrop, P. *Printed, Organic & Flexible Electronics Forecasts, Players & Opportunities 2015-2025*, 2015.

(2) Huang, Y.; Kramer, E. J.; Heeger, A. J.; Bazan, G. C. Bulk Heterojunction Solar Cells: Morphology and Performance Relationships. *Chem. Rev.* **2014**, *114*, 7006.

(3) Nagarjuna, G.; Venkataraman, D. Strategies for Controlling the Active Layer Morphologies in OPVs. *J. Polym. Sci. Pt. B-Polym. Phys.* **2012**, *50*, 1045.

(4) Dang, M. T.; Hirsch, L.; Wantz, G. P3HT:PCBM, Best Seller in Polymer Photovoltaic Research. *Adv. Mater.* **2011**, *23*, 3597.

(5) Chen, D.; Liu, F.; Wang, C.; Nakahara, A.; Russell, T. P. Bulk Heterojunction Photovoltaic Active Layers via Bilayer Interdiffusion. *Nano Lett.* **2011**, *11*, 2071.

(6) Moon, J. S.; Takacs, C. J.; Sun, Y. M.; Heeger, A. J. Spontaneous Formation of Bulk Heterojunction Nanostructures: Multiple Routes to Equivalent Morphologies. *Nano Lett.* **2011**, *11*, 1036.

(7) Treat, N. D.; Brady, M. A.; Smith, G.; Toney, M. F.; Kramer, E. J.; Hawker, C. J.; Chabinyc, M. L. Interdiffusion of PCBM and P3HT Reveals Miscibility in a Photovoltaically Active Blend. *Adv. Energy Mater.* **2011**, *1*, 82.

(8) Chen, D. A.; Nakahara, A.; Wei, D. G.; Nordlund, D.; Russell, T. P. P3HT/PCBM Bulk Heterojunction Organic Photovoltaics: Correlating Efficiency and Morphology. *Nano Lett.* **2011**, *11*, 561.

(9) Shaw, P. E.; Ruseckas, A.; Samuel, I. D. W. Exciton Diffusion Measurements in Poly(3-hexylthiophene). *Adv. Mater.* **2008**, *20*, 3516.

(10) Lee, J. K.; Ma, W. L.; Brabec, C. J.; Yuen, J.; Moon, J. S.; Kim, J. Y.; Lee, K.; Bazan, G. C.; Heeger, A. J. Processing Additives for Improved Efficiency from Bulk Heterojunction Solar Cells. *J. Am. Chem. Soc.* **2008**, *130*, 3619.

(11) Peet, J.; Kim, J. Y.; Coates, N. E.; Ma, W. L.; Moses, D.; Heeger, A. J.; Bazan, G. C. Efficiency Enhancement in Low-Bandgap Polymer Solar Cells by Processing with Alkane Dithiols. *Nat. Mater.* **2007**, *6*, 497.

(12) Gu, Y.; Wang, C.; Russell, T. P. Multi-Length-Scale Morphologies in PCPDTBT/PCBM Bulk-Heterojunction Solar Cells. *Adv. Energy Mater.* **2012**, *2*, 683.

(13) Liao, H. C.; Tsao, C. S.; Shao, Y. T.; Chang, S. Y.; Huang, Y. C.; Chuang, C. M.; Lin, T. H.; Chen, C. Y.; Su, C. J.; Jeng, U. S.; Chen, Y. F.; Su, W. F. Bi-Hierarchical Nanostructures of Donor-Acceptor Copolymer and Fullerene for High Efficient Bulk Heterojunction Solar Cells. *Energy Environ. Sci.* **2013**, *6*, 1938.

(14) Chen, W.; Xu, T.; He, F.; Wang, W.; Wang, C.; Strzalka, J.; Liu, Y.; Wen, J. G.; Miller, D. J.; Chen, J. H.; Hong, K. L.; Yu, L. P.; Darling, S. B. Hierarchical Nanomorphologies Promote Exciton Dissociation in Polymer/Fullerene Bulk Heterojunction Solar Cells. *Nano Lett.* **2011**, *11*, 3707.

(15) He, Z. C.; Zhong, C. M.; Su, S. J.; Xu, M.; Wu, H. B.; Cao, Y. Enhanced Power-Conversion Efficiency in Polymer Solar Cells Using an Inverted Device Structure. *Nat. Photonics* **2012**, *6*, 591.

(16) Hedley, G. J.; Ward, A. J.; Alekseev, A.; Howells, C. T.; Martins, E. R.; Serrano, L. A.; Cooke, G.; Ruseckas, A.; Samuel, I. D. W. Determining the Optimum Morphology in High-Performance Polymer-Fullerene Organic Photovoltaic Cells. *Nat. Commun.* **2013**, *4*, 10.

(17) Liao, H. C.; Ho, C. C.; Chang, C. Y.; Jao, M. H.; Darling, S. B.; Su, W. F. Additives for Morphology Control in High-Efficiency Organic Solar Cells. *Mater. Today* **2013**, *16*, 326.

(18) Jackson, N. E.; Savoie, B. M.; Marks, T. J.; Chen, L. X.; Ratner, M. A. The Next Breakthrough for Organic Photovoltaics? *J. Phys. Chem. Lett.* **2015**, *6*, 77.

(19) Nagarjuna, G.; Baghgar, M.; Labastide, J. A.; Algaier, D. D.; Barnes, M. D.; Venkataraman, D. Tuning Aggregation of Poly(3-hexylthiophene) within Nanoparticles. *ACS Nano* **2012**, *6*, 10750.

(20) Bartlett, P.; Ottewill, R. H.; Pusey, P. N. Superlattice Formation in Binary-Mixtures of Hard-Sphere Colloids. *Phys. Rev. Lett.* **1992**, *68*, 3801.

(21) Bartlett, P.; Ottewill, R. H.; Pusey, P. N. Freezing of Binary-Mixtures of Colloidal Hard-Spheres. *J. Chem. Phys.* **1990**, *93*, 1299.

(22) Shevchenko, E. V.; Talapin, D. V.; Kotov, N. A.; O'Brien, S.; Murray, C. B. Structural Diversity in Binary Nanoparticle Superlattices. *Nature* **2006**, *439*, 55.

(23) Chen, Z.; O'Brien, S. Structure Direction of II-VI Semiconductor Quantum Dot Binary Nanoparticle Superlattices by Tuning Radius Ratio. *ACS Nano* **2008**, *2*, 1219.

(24) Kietzke, T.; Neher, D.; Landfester, K.; Montenegro, R.; Guntner, R.; Scherf, U. Novel Approaches to Polymer Blends Based on Polymer Nanoparticles. *Nat. Mater.* **2003**, *2*, 408.

(25) Labastide, J. A.; Baghgar, M.; Dujovne, I.; Yang, Y. P.; Dinsmore, A. D.; Sumpter, B. G.; Venkataraman, D.; Barnes, M. D. Polymer Nanoparticle Super lattices for Organic Photovoltaic Applications. *J. Phys. Chem. Lett.* **2011**, *2*, 3085.

(26) Millstone, J. E.; Kavulak, D. F. J.; Woo, C. H.; Holcombe, T. W.; Westling, E. J.; Briseno, A. L.; Toney, M. F.; Frechet, J. M. J. Synthesis, Properties, and Electronic Applications of Size-Controlled Poly(3-hexylthiophene) Nanoparticles. *Langmuir* **2010**, *26*, 13056.

(27) Park, E. J.; Erdem, T.; Ibrahimova, V.; Nizamoglu, S.; Demir, H. V.; Tuncel, D. White-Emitting Conjugated Polymer Nanoparticles with Cross-Linked Shell for Mechanical Stability and Controllable Photometric Properties in Color-Conversion LED Applications. *ACS Nano* **2011**, *5*, 2483.

(28) Zhou, X. J.; Belcher, W.; Dastoor, P. Solar Paint: From Synthesis to Printing. *Polymers* **2014**, *6*, 2832.

(29) Chong, H.; Nie, C. Y.; Zhu, C. L.; Yang, Q.; Liu, L. B.; Lv, F. T.; Wang, S. Conjugated Polymer Nanoparticles for Light-Activated Anticancer and Antibacterial Activity with Imaging Capability. *Langmuir* **2012**, *28*, 2091.

(30) Fernando, L. P.; Kandel, P. K.; Yu, J. B.; McNeill, J.; Ackroyd, P. C.; Christensen, K. A. Mechanism of Cellular Uptake of Highly Fluorescent Conjugated Polymer Nanoparticles. *Biomacromolecules* **2010**, *11*, 2675.

(31) Wu, C.; Bull, B.; Szymanski, C.; Christensen, K.; McNeill, J. Multicolor Conjugated Polymer Dots for Biological Fluorescence Imaging. *ACS Nano* **2008**, *2*, 2415.

(32) Feng, L. H.; Zhu, C. L.; Yuan, H. X.; Liu, L. B.; Lv, F. T.; Wang, S. Conjugated Polymer Nanoparticles: Preparation, Properties, Functionalization and Biological Applications. *Chem. Soc. Rev.* **2013**, *42*, 6620.

(33) Pecher, J.; Huber, J.; Winterhalder, M.; Zumbusch, A.; Mecking, S. Tailor-Made Conjugated Polymer Nanoparticles for Multicolor and Multiphoton Cell Imaging. *Biomacromolecules* **2010**, *11*, 2776.

(34) Silva, A. T.; Alien, N.; Ye, C. M.; Verchot, J.; Moon, J. H. Conjugated Polymer Nanoparticles for Effective siRNA Delivery to Tobacco BY-2 Protoplasts. *BMC Plant Biol.* **2010**, *10*, 14.

(35) Pecher, J.; Mecking, S. Nanoparticles of Conjugated Polymers. *Chem. Rev.* **2010**, *110*, 6260.

(36) Tuncel, D.; Demir, H. V. Conjugated Polymer Nanoparticles. *Nanoscale* **2010**, *2*, 484.

(37) Landfester, K. The Generation of Nanoparticles in Miniemulsions. *Adv. Mater.* **2001**, *13*, 765.

(38) Landfester, K.; Montenegro, R.; Scherf, U.; Guntner, R.; Asawapirom, U.; Patil, S.; Neher, D.; Kietzke, T. Semiconducting Polymer Nanospheres in Aqueous Dispersion Prepared by a Miniemulsion Process. *Adv. Mater.* **2002**, *14*, 651.

(39) Keum, C. G.; Noh, Y. W.; Baek, J. S.; Lim, J. H.; Hwang, C. J.; Na, Y. G.; Shin, S. C.; Cho, C. W. Practical Preparation Procedures for Docetaxel-Loaded Nanoparticles Using Polylactic Acid-co-Glycolic acid. *Int. J. Nanomed.* **2011**, *6*, 2225.

(40) Wu, M.; Frochot, C.; Dellacherie, E.; Marie, E. Well-Defined Poly(butyl cyanoacrylate) Nanoparticles via Miniemulsion Polymerization. *Macromol. Symp.* **2009**, *281*, 39.

(41) Landfester, K.; Bechthold, N.; Tiarks, F.; Antonietti, M. Miniemulsion Polymerization with Cationic and Nonionic Surfactants: A Very Efficient use of Surfactants for Heterophase Polymerization. *Macromolecules* **1999**, *32*, 2679.

(42) Caruso, M. M.; Davis, D. A.; Shen, Q.; Odom, S. A.; Sottos, N. R.; White, S. R.; Moore, J. S. Mechanically-Induced Chemical Changes in Polymeric Materials. *Chem. Rev.* **2009**, *109*, 5755.

(43) May, P. A.; Moore, J. S. Polymer Mechanochemistry: Techniques to Generate Molecular Force via Elongational Flows. *Chem. Soc. Rev.* **2013**, *42*, 7497.

(44) Cravotto, G.; Gaudino, E. C.; Cintas, P. On the Mechanochemical Activation by Ultrasound. *Chem. Soc. Rev.* **2013**, *42*, 7521.

(45) Santos, H. M.; Lodeiro, C.; Capelo-Martínez, J.-L. In *Ultrasound in Chemistry*; Wiley-VCH Verlag GmbH & Co. KGaA: 2009, p 1.

(46) Capelo, J. L.; Galesio, M. M.; Felisberto, G. M.; Vaz, C.; Pessoa, J. C. Micro-Focused Ultrasonic Solid-Liquid Extraction (mu FUSLE) Combined with HPLC and Fluorescence Detection for PAHs Determination in Sediments: Optimization and Linking with the Analytical Minimalism Concept. *Talanta* **2005**, *66*, 1272.

(47) Filipe, V.; Hawe, A.; Jiskoot, W. Critical Evaluation of Nanoparticle Tracking Analysis (NTA) by NanoSight for the Measurement of Nanoparticles and Protein Aggregates. *Pharm. Res.* **2010**, *27*, 796.

(48) Tiwari, S.; Greenham, N. C. Charge Mobility Measurement Techniques in Organic Semiconductors. *Opt. Quantum Electron.* **2009**, *41*, 69.

(49) Huber, J.; Jung, C.; Mecking, S. Nanoparticles of Low Optical Band Gap Conjugated Polymers. *Macromolecules* **2012**, *45*, 7799.

(50) Szymanski, C.; Wu, C.; Hooper, J.; Salazar, M. A.; Perdomo, A.; Dukes, A.; McNeill, J. Single Molecule Nanoparticles of the Conjugated Polymer MEH-PPV, Preparation and Characterization by Near-Field Scanning Optical Microscopy. *The Journal of Physical Chemistry B* **2005**, *109*, 8543.

(51) Moon, J. H.; MacLean, P.; McDaniel, W.; Hancock, L. F. Conjugated Polymer Nanoparticles for Biochemical Protein Kinase Assay. *Chemical Communications* **2007**, 4910.

(52) Wu, C. F.; Bull, B.; Christensen, K.; McNeill, J. Ratiometric Single-Nanoparticle Oxygen Sensors for Biological Imaging. *Angew. Chem.-Int. Edit.* **2009**, *48*, 2741.

(53) Ye, F.; Wu, C.; Jin, Y.; Chan, Y.-H.; Zhang, X.; Chiu, D. T. Ratiometric Temperature Sensing with Semiconducting Polymer Dots. *J. Am. Chem. Soc.* **2011**, *133*, 8146.

(54) Moon, J. H.; Deans, R.; Krueger, E.; Hancock, L. F. Capture and Detection of a Quencher Labeled Oligonucleotide by Poly(phenylene ethynylene) Particles. *Chemical Communications* **2003**, 104.

(55) Wu, C. F.; Szymanski, C.; McNeill, J. Preparation and Encapsulation of Highly Fluorescent Conjugated Polymer Nanoparticles. *Langmuir* **2006**, *22*, 2956.

(56) Huebner, C. F.; Roeder, R. D.; Foulger, S. H. Nanoparticle Electroluminescence: Controlling Emission Color Through Förster Resonance Energy Transfer in Hybrid Particles. *Advanced Functional Materials* **2009**, *19*, 3604.

(57) Kietzke, T.; Neher, D.; Kumke, M.; Montenegro, R.; Landfester, K.; Scherf, U. A Nanoparticle Approach to Control the Phase Separation in Polyfluorene Photovoltaic Devices. *Macromolecules* **2004**, *37*, 4882.

(58) Venkataraman, D.; Yurt, S.; Venkatraman, B. H.; Gavvalapalli, N. Role of Molecular Architecture in Organic Photovoltaic Cells. *J. Phys. Chem. Lett.* **2010**, *1*, 947.

(59) Ballantyne, A. M.; Chen, L.; Dane, J.; Hammant, T.; Braun, F. M.; Heeney, M.; Duffy, W.; McCulloch, I.; Bradley, D. D. C.; Nelson, J. The Effect of Poly(3-hexylthiophene) Molecular Weight on Charge Transport and the Performance of Polymer:Fullerene Solar Cells. *Advanced Functional Materials* **2008**, *18*, 2373.

(60) Pingel, P.; Schwarzl, R.; Neher, D. Effect of Molecular p-Doping on Hole Density and Mobility in Poly(3-hexylthiophene). *Applied Physics Letters* **2012**, *100*, 143303.

(61) Shen, X.; Duzhko, V. V.; Russell, T. P. A Study on the Correlation Between Structure and Hole Transport in Semi-Crystalline Regioregular P3HT. *Adv. Energy Mater.* **2013**, *3*, 263.

(62) Salleo, A.; Kline, R. J.; DeLongchamp, D. M.; Chabinyc, M. L. Microstructural Characterization and Charge Transport in Thin Films of Conjugated Polymers. *Adv. Mater.* **2010**, *22*, 3812.

(63) Kim, J. S.; Lee, J. H.; Park, J. H.; Shim, C.; Sim, M.; Cho, K. High-Efficiency Organic Solar Cells Based on Preformed Poly(3-hexylthiophene) Nanowires. *Advanced Functional Materials* **2011**, *21*, 480.

(64) Newbloom, G. M.; Kim, F. S.; Jenekhe, S. A.; Pozzo, D. C. Mesoscale Morphology and Charge Transport in Colloidal Networks of Poly(3-hexylthiophene). *Macromolecules* **2011**, *44*, 3801.

(65) Landfester, K. In *Colloid Chemistry II*; Antonietti, M., Ed.; Springer Berlin Heidelberg: 2003; Vol. 227, p 75.

(66) Malliaras, G. G.; Shen, Y. L.; Dunlap, D. H.; Murata, H.; Kafafi, Z. H. Nondispersive Electron Transport in Alq(3). *Applied Physics Letters* **2001**, *79*, 2582.

(67) Hoffmann, S. T.; Jaiser, F.; Hayer, A.; Bässler, H.; Unger, T.; Athanasopoulos, S.; Neher, D.; Köhler, A. How Do Disorder, Reorganization, and Localization Influence the Hole Mobility in Conjugated Copolymers? *J. Am. Chem. Soc.* **2013**, *135*, 1772.

(68) Mauer, R.; Kastler, M.; Laquai, F. The Impact of Polymer Regioregularity on Charge Transport and Efficiency of P3HT:PCBM Photovoltaic Devices. *Advanced Functional Materials* **2010**, *20*, 2085.

(69) Choulis, S. A.; Kim, Y.; Nelson, J.; Bradley, D. D. C.; Giles, M.; Shkunov, M.; McCulloch, I. High Ambipolar and Balanced Carrier Mobility in Regioregular Poly(3-hexylthiophene). *Applied Physics Letters* **2004**, *85*, 3890.

(70) Sirringhaus, H.; Brown, P. J.; Friend, R. H.; Nielsen, M. M.; Bechgaard, K.; Langeveld-Voss, B. M. W.; Spiering, A. J. H.; Janssen, R. A. J.; Meijer, E. W.; Herwig, P.; de Leeuw, D. M. Two-Dimensional Charge Transport in Self-Organized, High-Mobility Conjugated Polymers. *Nature* **1999**, *401*, 685.

(71) Nicolaidis, N.; Vaughan, B.; Mulligan, C. J.; Bryant, G.; Zillger, T.; Trnovec, B.; Hubler, A. C.; Holmes, N.; Cooling, N. A.; Griffith, M. J.; Bilen, C.; Kumar, P.; Feron, K.; Zhou, X. J.; Elkington, D.; Belcher, W. J.; Dastoor, P. C. Solution Processable Interface Materials for Nanoparticulate Organic Photovoltaic Devices. *Applied Physics Letters* **2014**, *104*, 4.

(72) Chambon, S.; Schatz, C.; Sebire, V.; Pavageau, B.; Wantz, G.; Hirsch, L. Organic Semiconductor Core-Shell Nanoparticles Designed through Successive Solvent Displacements. *Mater. Horizons* **2014**, *1*, 431.

(73) Richards, J. J.; Whittle, C. L.; Shao, G. Z.; Pozzo, L. D. Correlating Structure and Photocurrent for Composite Semiconducting Nanoparticles with Contrast Variation Small-Angle Neutron Scattering and Photoconductive Atomic Force Microscopy. *ACS Nano* **2014**, *8*, 4313.

(74) Desmond, K. W.; Weeks, E. R. Random Close Packing of Disks and Spheres in Confined Geometries. *Phys. Rev. E* **2009**, *80*, 11.

(75) Borsenberger, P. M.; Pautmeier, L.; Bassler, H. Charge Transport in Disordered Molecular-Solids. *J. Chem. Phys.* **1991**, *94*, 5447.

(76) Darwis, D.; Holmes, N.; Elkington, D.; Kilcoyne, A. L. D.; Bryant, G.; Zhou, X. J.; Dastoor, P.; Belcher, W. Surfactant-free Nanoparticulate Organic Photovoltaics. *Sol. Energy Mater. Sol. Cells* **2014**, *121*, 99.

(77) Verploegen, E.; Mondal, R.; Bettinger, C. J.; Sok, S.; Toney, M. F.; Bao, Z. A. Effects of Thermal Annealing Upon the Morphology of Polymer-Fullerene Blends. *Advanced Functional Materials* **2010**, *20*, 3519.

(78) Zhao, J.; Swinnen, A.; Van Assche, G.; Manca, J.; Vanderzande, D.; Van Mele, B. Phase Diagram of P3HT/PCBM Blends and Its Implication for the Stability of Morphology. *J. Phys. Chem. B* **2009**, *113*, 1587.

(79) Trinh Tung, N.; Duc Nghia, N.; Van Tuyen, N. Glass Transition of PCBM, P3HT and Their Blends in Quenched State. *Advances in Natural Sciences: Nanoscience and Nanotechnology* **2012**, *3*, 045001.

(80) Ham, M. H.; Paulus, G. L. C.; Lee, C. Y.; Song, C.; Kalantar-zadeh, K.; Choi, W.; Han, J. H.; Strano, M. S. Evidence for High-Efficiency Exciton Dissociation at Polymer/Single-Walled Carbon Nanotube Interfaces in Planar Nano-heterojunction Photovoltaics. *ACS Nano* **2010**, *4*, 6251.

(81) Krebs, F. C. Polymer Solar Cell Modules Prepared Using Roll-to-Roll Methods: Knife-Over-Edge Coating, Slot-Die Coating and Screen Printing. *Sol. Energy Mater. Sol. Cells* **2009**, *93*, 465.

(82) Lu, G. H.; Bu, L. J.; Li, S. J.; Yang, X. N. Bulk Interpenetration Network of Thermoelectric Polymer in Insulating Supporting Matrix. *Adv. Mater.* **2014**, *26*, 2359.